Article:
Cosgrove, GIE, Colombera, L orcid.org/0000-0001-9116-1800 and Mountney, NP orcid.org/0000-0002-8356-9889 (2021) Quantitative analysis of the sedimentary architecture of eolian successions developed under icehouse and greenhouse climatic conditions. Geological Society of America Bulletin, 133 (11-12). pp. 2625-2644. ISSN 0016-7606

https://doi.org/10.1130/B35918.1

Title of manuscript: Quantitative analysis of the sedimentary architecture of eolian successions developed under icehouse and greenhouse climatic conditions

Grace I.E. Cosgrove[1], Luca Colombera[1], Nigel P. Mountney[1]

[1] *Fluvial & Eolian Research Group, School of Earth and Environment, University of Leeds, Leeds, LS2 9JT, UK*

ABSTRACT

The continental terrestrial record preserves an archive of how ancient sedimentary systems respond to and record changes in global climate. A database-driven quantitative assessment reveals differences in the preserved sedimentary architectures of siliciclastic eolian systems with broad geographic and stratigraphic distribution, developed under icehouse versus greenhouse climatic conditions. Over 5,600 geological entities, including architectural elements, facies, sediment textures and bounding surfaces, have been analyzed from 34 eolian systems of Paleoproterozoic to Cenozoic ages. Statistical analyses have been performed on the abundance, composition, preserved thickness, and arrangement of different eolian lithofacies, architectural elements and bounding surfaces. Results demonstrate that preserved sedimentary architectures of icehouse and greenhouse systems differ markedly. Eolian dune, sandsheet and interdune architectural elements that accumulated under icehouse conditions are significantly thinner relative to their greenhouse counterparts; this is observed across all basin settings, supercontinents, geological ages, and dune-field physiographic settings. However, this difference between icehouse and greenhouse eolian systems is exclusively observed for paleolatitudes <30°, suggesting that climate-induced changes in the strength and circulation patterns of trade winds may have partly controlled eolian sand accumulation. These changes acted in combination with variations in water-table levels, sand supply and sand transport, ultimately influencing the nature of long-term sediment preservation. During icehouse episodes, Milankovitch-cyclicity resulted in deposits typified by glacial accumulation and interglacial deflation. Greenhouse conditions promoted the accumulation of eolian elements into the geological record due to elevated water tables and biogenic and chemical stabilizing agents, which could protect deposits from wind-driven deflation. In the context of a rapidly changing climate, the results presented here can help predict the impact of climate change on Earth surface processes.

Keywords: Eolian, Database, Icehouse, Greenhouse, Climate

INTRODUCTION

The current rate of release of carbon dioxide into the atmosphere, largely through the anthropogenic combustion of fossil fuels, is occurring at a geologically unprecedented rate (Kidder and Worsley, 2011; Andrew, 2020; Peters et al., 2020). The associated changes in global climate, and the impact of such climate change in terms of its influence on Earth surface processes, has significant scientific and societal implications (e.g., IPCC, 2007 and references therein). Quantifying the response of Earth's geosphere to changes in climate therefore represents one of the foremost issues faced in modern sedimentology (Hodgson et al., 2018). Given the paucity of long-term (> 100 years) instrumental records, analysis of the sedimentary record is critical for understanding the impact of climate change on Earth surface processes. The continental terrestrial record preserves an archive of how ancient sedimentary systems respond to, and record, changes in global climate, over time scales far beyond the range of human experience. Observational evidence from the ancient sedimentary record therefore provides a means to both quantify past responses and predict future responses of the Earth's surface processes to shifts in global climate.

Throughout geological history, the Earth's climate can be subdivided into periods characterized by the presence or absence of major continental ice-sheets and polar ice (Fig. 1) – two climate states referred to as icehouse and greenhouse, respectively (Frakes et al., 1992; Price et al., 1998; Cromwell, 1999). The preserved eolian sedimentary record, which spans over three billion years of Earth history from the Archean to the present day (Clemmensen, 1985; Dott et al., 1986; Voss, 2002; Cather et al., 2008; Simpson et al., 2012; Rodríguez-López et al., 2014) is a valuable archive of the continental landscape response to periodic fluctuations between icehouse and greenhouse worlds.

A comprehensive global-scale quantitative comparison of the preserved architectures of sand-dominated eolian sedimentary systems (ergs, *sensu* Wilson, 1973) accumulated and preserved under icehouse and greenhouse conditions has not been undertaken previously. Prior research on this topic has been primarily reported in the form of largely qualitative accounts, commonly for individual case studies or regions from eolian successions associated with either greenhouse (e.g., Crabaugh and Kocurek, 1993; Kocurek et al., 1992; Jones and Blakey, 1997; Benan and Kocurek, 2000; Kocurek and Day, 2018) or icehouse (e.g., Cowan, 1993; Meadows and Beach, 1993; Clemmensen and Abrahamsen, 1983) climatic conditions.

In addition to the effects of climate, eolian sedimentary systems are sensitive to a variety of additional forcings, including rate and type of sediment supply, sea level, tectonic configuration, basin setting and dune-field physiographic setting (e.g., Blakey and Middleton, 1983; Blakey, 1988; Mountney et al., 1999; Kocurek et al., 2001; Nichols, 2005; Soria et al., 2011). As such, isolating and quantifying the global effects of climate as a control on sedimentary systems is difficult, especially for individual case studies. To address this problem, this study uses a global dataset derived from 42 published articles associated with 34 ancient eolian successions (Fig. 1).

The aim of this study is to quantify relationships between global climate states and preserved eolian sedimentary architecture at multiple scales of observation. This study addresses three main research questions: (i) How are the characters of preserved eolian and related architectural elements, and their bounding surfaces affected by fluctuations in global climate states? (ii) Does the prevailing global climate influence the sedimentology and stratigraphic architecture of preserved eolian sedimentary successions? (iii) Can the effects of icehouse and greenhouse conditions on preserved eolian sedimentary architectures be isolated from those of supercontinental setting, paleolatitude, basin setting and dune-field physiographic setting?

Background: an Overview of the Icehouse and Greenhouse Earth

Icehouse and greenhouse conditions account for approximately 15% and 85% of Earth history, respectively (Fig. 1; Frakes et al., 1992; Crowell, 1999; Link, 2009). Global shifts between icehouse and greenhouse conditions are caused by the cumulative effects of astronomical, biogeochemical and tectonic events, which interact with each other and lead to the development of feedback mechanisms that act to influence global climate. Icehouse and greenhouse conditions are respectively defined by the presence or absence of major polar ice-sheets that calve marine icebergs (Kidder and Worsley, 2012). Greenhouse conditions can, however, be associated with seasonal sea ice, alpine glaciers and transient polar ice-caps (Frakes, 1992; Kidder and Worsley, 2012).

Five major icehouse periods are recognized in Earth history (Fig. 1): the Huronian (2400-2100 Ma; Coleman, 1907; Evans et al., 1997), the Cryogenian (720-635 Ma; Knoll and Walter, 1992; Bowring et al., 2003; Hoffman et al., 2004), the Late Ordovician and Early Silurian glaciations, also known as the Andean-Saharan (450-420 Ma; Brenchley et al., 1994), the Late Paleozoic (360-260 Ma; Montanez and Poulsen, 2013; Goddéris et al., 2017), and the current Cenozoic icehouse conditions that persist today (since 33.9 Ma; Frakes et al., 1992). The five major icehouse intervals have each lasted for tens of millions of years and are each associated with mid-latitude glaciation down to sea level (Frakes et al., 1992; Cromwell, 1999). Relative to greenhouse conditions, icehouse conditions are typically associated with: (i) lower atmospheric levels of carbon dioxide; (ii) lower sea levels and sea-surface temperatures; (iii) strong thermohaline deep-ocean circulation; (iv) strong marine polar-to-equatorial thermal contrasts; (v) increased wind velocities at low-latitudes (< 30º) leading to higher wind shear and higher wind-related erosive power (Fig 2; Frakes et al., 1992; Cromwell, 1999; Forster et al., 2007; Kidder and Worsley, 2010, 2012).

Within long-lived icehouse periods, climatic conditions are known to fluctuate between glacial and interglacial episodes, which give rise to the waxing and waning of continental glaciations; these cycles of glacial expansion and retreat are superimposed onto overall longer-term net icehouse conditions. In the most recent Cenozoic icehouse, glacial and interglacial cycles occur at quasi-100 kyr intervals, with shorter 41 kyr and 21 kyr quasi-cycles superimposed (Shackleton et al., 1999). The cyclic regularity of glacial and interglacial periods is attributed dominantly to variations in the Earth's orbital parameters – the so-called Milankovitch cyclicity. The effects on the sedimentation of glacial and interglacial oscillations are well documented in the deep-sea sedimentary record (e.g., Rea and Janeck, 1981; Hovan et al., 1991; Petit et al., 1991; Winckler et al., 2008). For example, eolian dust supply to the deep sea is greater under glacial conditions, relative to interglacial conditions (e.g., Woodard et al., 2011), as a consequence of heightened aridity and stronger wind strengths during glacial episodes.

METHODOLOGY

Case Studies and Associated Metrics

Thirty-four case studies, each representing an ancient eolian sedimentary succession (Fig. 1, Table 1), and associated with detailed datasets from 42 published articles, have been analyzed using the Database of Aeolian Sedimentary Architecture (DASA). DASA is a relational database that stores data on a variety of eolian and associated non-eolian entities relating to different scales, including architectural elements, lithofacies and bounding surfaces. DASA records both qualitative and quantitative attributes that characterize the type, geometry, spatial relations, hierarchical relations, temporal significance, and textural and petrophysical properties of eolian and related depositional units and their bounding surfaces. In this study, architectural elements, facies elements, textural properties and eolian bounding-surface types documented from the selected case-study examples are analyzed.

For this investigation, of the 42 scientific articles considered, 24 provide accounts of systems developed under icehouse conditions and 18 of greenhouse systems. Of the 34 case studies, 20 represent icehouse conditions and 14 represent greenhouse conditions. In total, 5,598 geological entities representing architectural and facies elements, textural observations and eolian bounding surfaces have been analyzed: 2,772 relate to sedimentary successions interpreted as having accumulated under the influence of icehouse climatic conditions; 2,826 under greenhouse conditions. Observations can be further categorized as follows: (i) 2,578 eolian and associated non-eolian architectural elements have been analyzed, of which 1,156 and 1,422 architectural elements relate to icehouse and greenhouse case-study systems, respectively; (ii) 985 eolian facies units have been analyzed, of which 630 and 355 facies relate to icehouse and greenhouse case-study systems, respectively; (iii) 1,308 textural observations have been analyzed, of which 749 and 559 relate to icehouse and greenhouse case-study systems, respectively; (iv) 727 bounding surfaces have been analyzed, of which 237 and 490 relate to icehouse and greenhouse systems, respectively.

Each examined case study has associated metadata describing its geological background and the boundary conditions present at the time of deposition; these metadata include the prevailing climate, basin setting, geologic age and paleosupercontinental setting. Metadata are derived from the original source work and additional published literature.

Architectural elements are defined as distinct sedimentary bodies with characteristic sedimentological properties (e.g., internal composition, geometry), and are the products of deposition in a specific sub-environment (e.g., a dune, a wet interdune, or a fluvial channel; for definitions see Table 2). Facies elements are defined as sedimentary bodies differentiated on the basis of sediment composition, texture, structure, bedding geometry, fossil content, or by the nature of their bounding surfaces (cf. Colombera et al., 2012, 2016).

At the scale of architectural and facies elements, each element is assigned an interpretation derived from the original source work (e.g., a dune set at the architectural-element scale, or adhesion strata at the facies-element scale). For each architectural and facies element, geometric properties (element thickness, length and width) are also recorded. However, in this investigation, the only geometric parameter considered in detail is the thickness of the deposit.

The textural properties considered here are grain size, sorting and roundness. For all textural properties, if a numerical value is not assigned in the original source work, but a descriptive term is provided (e.g., fine-grained sand), classes are converted into numerical values according to the schemes of Folk and Ward (1957) for grain size and sorting, and to the Krumbein scale of roundness (Krumbein, 1941).

The following types of qualitative data regarding super-bounding surfaces (supersurfaces) are considered here: (i) a classification of surface type (i.e., environmental significance) according to the schemes of Fryberger (1993) and Kocurek (1996); (ii) the association of features (sedimentary structures) indicative of substrate conditions (e.g., dry, damp, wet) and associated with the state of the surface; and (iii) the occurrence of features indicative of surface stabilization (e.g., Ahlbrandt et al., 1978; Loope, 1988; Basilici et al., 2009, 2020; Dal' Bo et al., 2010; Krapovickas et al., 2016).

Dating Ancient Eolian Successions

Ancient eolian successions can be difficult to date in absolute terms due to a general paucity of features suitable for numerical age-dating (Rodríguez-López et al., 2014). As such, determining the time when an eolian succession accumulated can be challenging. Some eolian deposits closely associated with (i) extrusive volcanics, (ii) fossil-rich marine interbeds, or (iii) abundant micro-fossils present in the eolian deposits themselves, can be dated and assigned a geochronometric or biostratigraphic age. More commonly, however, only a relative age can be established, such that eolian successions might be interpreted in terms of sequence-stratigraphic or climate-stratigraphic contexts (e.g., Mountney and Howell, 2000; Atchley and Loope, 1993; Jordan and Mountney, 2010, 2012). Many eolian successions contain surfaces that are thought to represent and record multiple long-lived depositional hiatuses in accumulation, associated with the formation of supersurfaces (e.g., Loope, 1985). For many eolian systems, the amount of time represented by such supersurfaces is likely significantly greater than that represented by the eolian accumulations themselves; eolian successions may be representative of only a small amount of the total geological time over which the eolian system was active (Loope, 1985; cf. Ager, 1993; Sadler, 1981). The preserved sedimentary record of eolian systems is highly fragmentary and age ranges of eolian deposits reported in the literature may be over- or under-estimates; accurately determining the ages of ancient eolian successions represents therefore an unavoidable caveat.

For this analysis, examined case studies have been assigned to a binary ‘icehouse’ or ‘greenhouse’ classification scheme. Despite the above-discussed limitations on dating eolian successions, given that major icehouse and greenhouse episodes span (many) tens of millions of years, placing eolian successions within in an ‘icehouse’ or ‘greenhouse’ category can be achieved with confidence; this study requires only that the age-range of each eolian succession considered in the analysis generally falls within episodes classed as icehouse or greenhouse climate states (Frakes et al., 1992; Crowell, 1999; Link, 2009). As such, precise absolute ages for eolian successions considered in this analysis are not crucial.

Determining the age-ranges of Precambrian eolian successions can, however, be more challenging, since their ages are typically more difficult to constrain (e.g., Pulvertaft, 1985; Simpson et al., 2012) and they cannot necessarily be reliably assigned to an ‘icehouse’ or ‘greenhouse’ climate category. Only Precambrian eolian successions with age-ranges that fall into to an ‘icehouse’ or ‘greenhouse’ category have been included in the analysis. In the analysis and discussion all Precambrian icehouse examples are compared against all Precambrian greenhouse examples.

There also exist eolian successions that record evidence of system development in a transitional state between icehouse and greenhouse worlds (see Eriksson et al., 2019). Such examples cannot readily be assigned to the binary icehouse-greenhouse classification scheme used in this study. Given that the focus of this study on the eolian sedimentary signature of climate extremes, examples of these “transitional" eolian successions have not been included in this investigation.

Carbonate Eolian Systems

In this investigation, siliciclastic-dominated eolian successions have been studied; carbonate-dominated eolian successions are not considered. Carbonate-dominated eolian successions (eolianites) most commonly develop along humid, mid-high latitude coasts, and along arid to semi-arid, mid-low latitude coasts that neighbor carbonate platforms (Clemmensen et al., 1997; Brooke, 2001; Nielsen et al., 2004; Simpson et al., 2004; Frébourg et al., 2008; Fornós et al., 2009; Andreucci et al., 2010). Carbonate-dominated eolian successions commonly undergo early post-depositional modification, notably via the precipitation of early diagenetic calcitic cements, which can readily stabilize original dune topography (Pye, 1983; Simpson et al., 2004; Guern and Davaud, 2005). As such, processes of deflation, construction, accumulation and preservation in carbonate eolian systems are markedly different to those of most siliciclastic eolian systems. In particular, dune deflation can be retarded, and dune stabilization and accumulation can be enhanced by early diagenetic cementation. Mechanisms of preservation of carbonate-dominated eolian deposits in relation to prevailing climatic and sediment supply conditions differ considerably from those of siliciclastic-dominated systems (Rodríguez-López et al., 2014). For these reasons, this study only considers siliciclastic-dominated eolian systems and their deposits.

Statistical Analysis

Quantitative data, including element thickness, grain size, sorting and grain roundness have been subject to statistical analysis. One-tail t-tests have been undertaken to determine if a significant difference exists between the means of icehouse and greenhouse groups. To test for statistical significance of differences among multiple groups (i.e. for the example considering multiple supercontinents under greenhouse conditions), analysis of variance (ANOVA) is applied. Post-hoc tests, using a Bonferroni correction, are applied to t-tests and ANOVA tests alike. An α value of 0.05 is considered for all statistical analyses; a family-wise alpha is considered when applying the Bonferroni correction.

RESULTS

Table 3 provides a summary of results of statistical analyses discussed in the text; this includes mean, median, standard deviation, and number of observations for variables of interest (eolian and related element thicknesses, grain size, sorting and roundness), and the results of statistical tests. In the text, for brevity only mean values are reported.

Eolian Elements

Differences in the characteristics of eolian and associated non-eolian architectural elements are considered first (Table 2). The relative proportion of types of eolian and non-eolian architectural elements is determined based on total element counts: eolian architectural elements form 63% and 62% of architectural elements in the studied successions accumulated under icehouse and greenhouse conditions, respectively (Fig. 3A). For all architectural elements classified as 'eolian' (Table 2), statistically significant differences in element thickness are found; icehouse eolian architectural elements are significantly thinner than greenhouse eolian elements, with mean values of element thickness of 2.36 m and 5.47 m, respectively (Fig. 4A; Table 3).

Of the total recorded eolian architectural elements, the percentages of elements classified as 'dune set', 'sandsheet' and 'interdune' are considered further (Fig. 3B; for definitions see Table 2). Dune sets form 62% and 82% of all recorded observations for icehouse and greenhouse eolian successions, respectively (Fig. 3B). Sandsheets form 20% and 12% of icehouse and greenhouse eolian successions, respectively (Fig. 3B). Interdunes form 18% and 4% of the icehouse and greenhouse successions, respectively (Fig. 3B). All three major eolian architectural element types (dune sets, sandsheets and interdunes) show statistically significant differences in mean element thickness (Fig. 4B-D; Table 3). Under icehouse conditions, dune sets, sandsheets and interdunes have mean thicknesses of 3.67 m, 0.55 m and 0.88 m, respectively (Table 3). Under greenhouse conditions, dune sets, sandsheets and interdunes have mean thicknesses of 5.93 m, 4.15 m and 2.00 m, respectively (Fig. 4B-D; Table 3).

Interdune elements are considered further and subdivided into 'wet', 'damp', and 'dry' types (*sensu* Kocurek, 1981) (Fig. 5A; for definitions see Table 2). In successions developed under icehouse conditions, 15% of interdune elements are of wet type, 48% are of damp type, and 37% are of dry type. In greenhouse successions, 60% of interdune elements are of wet type, 30% are of damp type, and 10 % are of dry type (Fig. 5A).

Non-Eolian Architectural Elements

The percentage of recorded non-eolian architectural elements reported for the studied successions is similar across icehouse and greenhouse successions, forming 37% and 38% of recorded observations, respectively (Fig. 3C). Under both icehouse and greenhouse conditions, alluvial and fluvial deposits are the most common non-eolian element types. Greenhouse successions are associated with a greater percentage of sabkha elements (14% vs 1%). Across icehouse and greenhouse successions, there is no statistically significant difference in the mean thickness of non-eolian architectural elements of any type (Table 3).

Eolian Facies Elements

In greenhouse successions, interdune elements of any type are most likely composed of adhesion strata (92%) and plane-bed lamination (8%) (Fig. 5B). In icehouse successions, a greater variety of facies-element types are recorded, including adhesion strata (38%), subaqueous ripples (27%), plane-bed lamination (19%), wind-ripple lamination (14%) and deflation-lag strata (2%). Icehouse sandsheet elements are dominated by adhesion strata (30%), deflation-lag strata (28%) and wind-ripple strata (27%), whereas greenhouse sandsheet elements mostly comprise wind-ripple strata (61%) and interfingered strata (30%) (Fig. 5C; interfingered strata comprise intercalated deposits of wind-ripple, grainflow, grainfall and/or plane-bed strata in varying proportions – Table 2). In icehouse successions, facies elements of any type are significantly thinner than those in greenhouse successions (mean thickness of 2.20 m vs 7.53 m; Fig. 4E; Table 3). For descriptions of facies units see Table 2.

Eolian Texture

The textural properties of all eolian architectural and facies elements are now considered. Systems developed under icehouse and greenhouse conditions have mean values of modal grain size of 0.34 mm and 0.36 mm (both medium sand; Fig. 6A); the difference between these values is not statistically significant (Table 3).

Icehouse systems are characterized by a higher median value of modal grain size of 0.38 mm (medium sand), relative to 0.25 mm (fine-to-medium sand) for greenhouse systems (Fig. 6A).

In both icehouse and greenhouse systems, eolian sands are, on average, moderately well sorted (icehouse = 0.57 σ, greenhouse = 0.58 σ; Fig. 6B); there is no statistically significant difference between mean values of sorting (Table 3). There is, however, a statistically significant difference in mean values of grain roundness between icehouse (mean = 0.57 K: rounded) and greenhouse (mean = 0.77 K: well-rounded) eolian sands (Fig. 6C) (Table 3). Thus, greenhouse conditions are associated with increased sand-grain textural maturity relative to icehouse conditions.

Eolian Surfaces

Eolian supersurfaces are recorded from 12 systems; 6 each represent icehouse and greenhouse conditions.

Supersurface Spacing

The average supersurface spacing is calculated by measuring the vertical distance between two successive supersurfaces. Under icehouse conditions the mean spacing is 16.34 m (standard deviation = 12.70 m; Table 3); under greenhouse conditions the mean spacing in 9.07 m (standard deviation = 6.34 m; Table 3). This indicates that supersurfaces are more widely spaced under icehouse conditions relative to greenhouse conditions; however, icehouse supersurfaces exhibit greater variability in supersurface spacing.

Supersurface Descriptions

Supersurfaces present in icehouse successions are classified dominantly as deflationary (88%) and subordinately as bypass surfaces (12%) (Fig. 7A). In greenhouse systems, deflationary and bypass supersurfaces form 67% and 33% of recorded supersurfaces, respectively (Fig. 7A). The nature of the substrate associated with the supersurfaces also varies considerably between icehouse and greenhouse examples. Icehouse supersurfaces are dominantly associated with features indicative of a wet surface (86%) and only rarely of a damp (6%) or dry (8%) surface. By contrast, in greenhouse successions, dry, damp and wet surface types are associated with 12%, 24% and 64% of recorded supersurfaces, respectively (Fig. 7B). When the nature of stabilization of supersurfaces is considered, 62% of icehouse supersurfaces are classified as unstabilized and 38% as stabilized; for greenhouse conditions, unstabilized and stabilized supersurfaces comprise 85% and 15% of recorded supersurfaces, respectively (Fig. 7C).

Non-Climatic Controls

In addition to climate, other controls might influence the preserved style and geometry of sedimentary architectures in eolian systems (e.g., Blakey and Middleton, 1983; Blakey, 1988; Mountney et al., 1999; Kocurek et al., 2001; Nichols, 2005; Soria et al., 2011). To better discriminate the influence of icehouse and greenhouse conditions, these other factors must be considered. To this end, where data are available, comparisons between icehouse and greenhouse conditions are made for: (i) specific paleogeographical configurations and geological age, (ii) basin setting, (iii) paleolatitude, and (iv) dune-field (erg) physiographic setting. In the following analyses, the thicknesses of eolian architectural elements (cross-strata packages, dune sets, dune cosets, dune compound sets, sandsheets and interdunes) are considered.

Paleogeography and Geological Age

Two supercontinental paleogeographic configurations spanned both icehouse and greenhouse times: those associated with Precambrian supercontinents (Rodinia and Columbia), and Pangea; the number of case studies falling into these categories are 6 and 11, respectively. When evaluated separately for the Precambrian and Pangean supercontinental settings, statistically significant differences between the mean thickness of eolian architectural elements deposited under icehouse and greenhouse conditions are seen (Table 3). The mean thickness of Precambrian architectural elements is 1.43 m and 5.03 m for icehouse and greenhouse successions, respectively (Fig. 8A), whereas the mean thickness of Pangean architectural elements is 3.41 m and 6.85 m for icehouse and greenhouse conditions, respectively (Fig. 8A; Table 3).

Basin Setting

Of the case-study examples examined in this study, eolian systems deposited under icehouse and greenhouse conditions are both recognized in the infill of sedimentary basins classified as intracratonic (sag) basins, continental rifts, and foreland basins (for definitions see Table 2); the number of case studies falling into these categories are 17, 4, and 3, respectively. For each of these basin types, there exists a statistically significant difference between the mean values of the thicknesses of eolian architectural elements deposited under icehouse and greenhouse conditions (Table 3). Architectural elements accumulated under icehouse conditions in intracratonic, rift and foreland basins yield mean thickness values of 1.73 m, 0.70 m and 2.11 m, respectively (Fig. 8B). Greenhouse architectural elements in intracratonic, rift and foreland basins instead return mean thickness values of 7.63 m, 2.48 m and 4.23 m, respectively (Fig. 8B; Table 3).

Paleolatitude

Paleolatitudes of eolian systems in this study are subdivided into the following categories: 0-15°, 16-30°, 31-45°, and 46-60°; the number of case studies falling into these categories are 11, 12, 5, and 4, respectively. A statistically significant difference is seen between icehouse and greenhouse eolian architectural element thicknesses for both paleolatitude ranges of 0-15° and 16-30° (Table 3). The mean thickness of eolian architectural elements deposited in paleolatitudes of 0-15° are 2.60 m and 6.38 m for icehouse and greenhouse systems, respectively (Fig. 8C, 9). The mean thickness of eolian architectural elements deposited in paleolatitudes of 16-30° are 2.72 m and 6.40 m for icehouse and greenhouse systems, respectively (Fig. 8C, 9). However, for systems from paleolatitudes >30°, no statistically significant difference is seen in mean eolian architectural element thickness (Table 3).

Dune-Field (Erg) Physiographic Setting

Major sand seas (ergs) can be subdivided into three generalized environmental sub-components: back-, central- and fore-erg (*sensu* Porter, 1986); the number of case studies falling into these categories are 8, 10, and 4, respectively. When these three dune-field settings are separately analyzed, a statistically significant difference in mean eolian architectural element thickness is observed in each erg-setting between icehouse and greenhouse conditions (Table 3). Back-erg settings record mean eolian architectural element thicknesses of 1.65 m and 2.92 m for icehouse and greenhouse conditions, respectively (Fig. 8D). Central-erg settings record mean eolian architectural element thicknesses of 3.39 and 12.83 m for icehouse and greenhouse conditions, respectively (Fig. 8D). Fore-erg settings record mean eolian architectural element thicknesses of 1.87 m and 6.36 m for icehouse and greenhouse conditions, respectively (Fig. 8D).

DISCUSSION

Prevailing climatic conditions influence the caliber of sediment and the rate of its supply, sediment availability for eolian transport, water-table fluctuations, and wind regimes (variability and strength), all of which themselves control resultant eolian sedimentary architecture (Kocurek, 1998; Clarke and Rendell, 1998; Mountney et al., 1999; Nichols, 2005). The observed differences in preserved eolian-element thickness are interpreted to arise from the prevailing climatic conditions associated with icehouse and greenhouse worlds. The relative thicknesses of eolian successions are also dependent on the availability of accommodation, and the rate at which it is created whilst a system is active. Different basin-types are associated with variable rates of accommodation generation (Gregory, 1894; Rosendahl, 1987; Middleton, 1989; Schlische, 1993; Einsele, 2013); the effects of basin type and accommodation is discussed in section '***Basin Configuration***' below.

Icehouse Conditions

When dune sets, sandsheets and interdunes are considered, all are significantly thinner in successions accumulated under icehouse conditions, relative to those relating to greenhouse conditions. Icehouse conditions are associated with orbitally controlled oscillations (Milankovitch cycles: Milankovitch, 1941; Wanless and Shepard, 1936; Dickinson et al., 1994) between drier and windier glacials, favoring eolian-dune construction (Loope, 1985; Mountney, 2006) – and more humid interglacials, favoring dune deflation (Rea and Janeck, 1981; Hovan et al., 1991; Petit et al., 1991; Kocurek, 1999; Kocurek and Lancaster, 1999; Winckler et al., 2008; Woodard et al., 2011). The observation of consistently thinner eolian deposits in the icehouse stratigraphic record, relative to their greenhouse counterparts, is attributed to the interactions between these constructive and destructive phases, which operate on timescales of ca. 100-400 kyr (Wanless and Shepard, 1936; Loope, 1985; Dickinson et al., 1994).

A Sequence of Eolian Accumulation and Deflation

Eolian accumulation and deflation during icehouse times can be described as follows. Globally, shifts from interglacial to glacial periods tend to be associated with the establishment of more arid conditions, an increase in wind speeds at trade-wind latitudes, and a relative fall in the level of regional water tables (Figs. 2, 10A; Rea and Janeck, 1981; Hovan et al., 1991; Petit et al., 1991; Winckler et al., 2008; Woodard et al., 2011). During the initial phase of glacial waxing and associated marine regression (i.e. equivalent to a falling-stage systems tract; Plint and Nummedal, 2000), large volumes of sediment are made available for potential eolian transport due to the exposure of areas of the continental shelf, and due to water-table falls that favor the eolian remobilization of continental deposits (Loope, 1985; Kocurek et al., 2001). The combination of an increase in the availability of sediment for eolian transport and an increase in the potential sand-carrying capacity of the wind brought about by increased wind velocity promotes an initial phase of eolian system construction and accumulation (Kocurek, 1999; Kocurek and Lancaster, 1999). At this stage, accumulating eolian systems tend to be dominated by sandsheets, associated with intermittent high-speed wind conditions (Clemmensen, 1991), and by relatively thin dune sets, produced by the repeated cannibalization of trains of dunes climbing at relatively low angles (Fig. 10A; Mountney, 2006). Thus, sandsheets are expected to form a significantly greater percentage (20% vs 12%) of observed icehouse eolian elements, relative to greenhouse successions.

As glacial conditions continue (at a time equivalent to that of the lowstand systems tract; cf. Van Wagoner et al., 1990), the increasing aridity drives a further lowering of the water table and the progressive loss of vegetation (in eolian systems deposited after the evolution of vascular land plants). This leads to the exposure of even larger sediment volumes, which are made available for entrainment and transport by strong trade winds with high sediment-carrying capacities (Kocurek, 1998). The relative increase in aridity and windiness controls both the availability of sediment for eolian transport and the transport capacity of the wind (Fig. 2; cf. Sarnthein 1978; Anton 1983; Mainguet and Chemin 1983; Lancaster 1989, 1990; Kocurek and Lancaster, 1999). Given these conditions, eolian sediment transport (flux) is large. As sand-saturated air decelerates within a sedimentary basin in which unfilled accommodation is available, large volumes of sand may be deposited rapidly; this promotes the accumulation of thicker dune-sets, relative to those deposited at the onset of an eolian accumulation episode (Fig. 10B; Wilson, 1971, 1973; Middleton and Southard, 1984; Kocurek, 1991; Mountney, 2006). However, the ultimate preservation potential of these thicker dune-sets may be relatively limited (see below).

As a glacial episode continues further, the upwind supply of sand is eventually exhausted (Loope, 1985; Mountney, 2006). An upwind exhaustion of the sediment supply results in the under-saturation of the airflow with respect to its potential sand-carrying capacity. This, in combination with the highly erosive trade winds (which can be up to 60% more erosive than they are under greenhouse conditions; Fig. 2; Kidder and Worsley, 2010, 2012) causes a switch to net deflationary conditions around a time of maximum aridity when water tables are low (Fig. 10C; Loope, 1985; Rubin and Hunter, 1982; Kocurek and Havholm, 1993; Kocurek, 1999). Erosional conditions result in the commencement of erg deflation and destruction (Wilson, 1973; Pye and Lancaster, 2009; Mountney, 2006; Bállico et al., 2017).

During the initial phase of glacial waning and associated onset of marine transgression, eolian deflation of the dune-sets comprising the uppermost units of an accumulated eolian succession continues (Fig. 10D; timing equivalent to that of the transgressive systems tract; cf. Van Wagoner et al., 1990). The onset of interglacial conditions is associated with a relative rise in sea level, a rise in the water table and re-colonization of the accumulation surface by vegetation. Cumulatively, these factors, in combination with weakened trade-wind strengths, reduce the volume of sediment susceptible to deflation, and the sediment transport capacity of the wind (Kocurek, 1991; Mountney, 2006). Water tables rise above the level of the thin dune sets and sandsheet deposits forming the lower parts of glacial eolian successions (Fig. 10D), thereby enhancing their long-term preservation potential.

As the interglacial proceeds (timing equivalent to that of the highstand systems tract; cf. Van Wagoner et al., 1990), the strength of trade winds continues to decrease (Fig. 2). The overall reduction in both sediment-transport capacity and sediment supply rates make interglacial eolian systems both supply- and transport-limited (cf. Kocurek and Lancaster, 1999). Deflation progresses to the level of the water table (Stokes, 1968), generating a supersurface (equivalent to a sequence boundary; cf. Van Wagoner et al., 1990), potentially associated with surface stabilization resulting from colonization by vegetation or microbial communities, by chemical precipitates, or by fluvial inundation (Fig. 10D; Loope, 1988; Kocurek, 1991; Dott, 2003; Basilici et al., 2009, 2020; Eriksson et al., 2000; Dal' Bo et al., 2010; Simpson et al., 2013). The timing of eolian supersurface formation can span a protracted length of time, and its culmination can vary in timing from late in a glacial episode to a point of maximum humidity during an ensuing interglacial episode (i.e. associated with the highstand systems tract). Thus, the timing of supersurface formation may contrast with that of sequence boundary formation in marine environments, which typically occurs during the falling-stage and early lowstand systems tracts (cf. Mitchum, 1977).

As the interglacial continues, eolian accumulation remains limited. This is due to the cumulative effects of elevated water tables and increased vegetation cover (in eolian systems deposited after the evolution of vascular land plants), which act to limit sediment availability (Fryberger et al., 1990; Kocurek and Havholm, 1993; Kidder and Worsley, 2010), and weaker wind strengths, which act to limit sediment transport capacity (Kocurek, 1999). This cycle of eolian accumulation recommences when climatic conditions tip back into windier, more arid glacial conditions (Fig. 10E-G).

The process of deflation preferentially erodes the lager dune sets occurring in the upper part of eolian successions that accumulated during glacial episodes; the thinner dune-sets and sandsheets forming the lower parts of such successions are less prone to deflation, since the concomitant rise in the water table can lead to their permanent preservation in the stratigraphic record (Fig. 10D; Kocurek and Havholm, 1993; Mountney and Russell, 2009; Mountney 2006). The preservation of relatively thicker dune-sets, associated with peak aridity during glacial times, may be limited to times and tectonic contexts of rapid subsidence. On the basis of this evolutionary model, the significantly reduced thickness of icehouse – relative to greenhouse – eolian architectural elements (i.e. dune-sets, sandsheets and interdunes) in the geological record is explained by their reduced preservation potential over Milankovitch timescales (100-400 kyr).

Icehouse Deflation

During icehouse glacial episodes, generally more arid landscapes are associated with relatively depressed water tables. As such, accumulating eolian successions are less likely to be permanently sequestered beneath the water table, and are therefore prone to deflation by strengthened low-latitude trade winds (Kocurek and Havholm, 1993). Such episodes are also generally associated with a reduced presence of stabilizing agents on the Earth's surface (e.g., vegetation and biogenic and evaporitic crusts), leaving eolian deposits exposed to potential erosion (Loope, 1988; Kocurek, 1991; Basilici et al., 2009, 2020; Dal' Bo et al., 2010).

The propensity of icehouse conditions to drive significant wind erosion following the cessation of eolian accumulation is supported by the dominance of deflationary supersurfaces, which are more common under icehouse conditions, relative to greenhouse conditions (deflationary supersurfaces represent 88% and 67% of classified supersurfaces in icehouse and greenhouse systems, respectively). The formation of deflationary supersurfaces with associated wet-surface features indicates that conditions of net accumulation are related to cyclic changes to net-erosional conditions, associated with eolian cannibalization and deflation down to the water table (Stokes, 1968; Loope, 1985; Mountney and Jagger, 2004; Mountney, 2006). This is the case for the icehouse Cedar Mesa Sandstone and many other Permo-Carboniferous deposits across North America, in which erg sequences are capped by regionally extensive deflationary, supersurfaces with associated sedimentary structures that indicate deflation to the paleo-water table (Loope, 1985; Fryberger, 1993; Mountney and Jagger, 2004; Mountney, 2006).

Greater rates of eolian winnowing under icehouse conditions are indicated by the higher number of observations of sandsheet elements. Sandsheets can represent remnants of eroded landforms of originally higher relief; their occurrence can reflect eolian deflation, whereby the winnowing of finer-grained sand leaves behind a coarser lag (Nielsen and Kocurek, 1986; Pye and Tsoar, 1990; Mountney and Russell, 2004, 2006). It is therefore significant that deflationary lag strata form a common facies type in icehouse sandsheet deposits, but are a comparatively rare component of greenhouse sandsheet deposits. The evidence of heightened eolian deflation of sandsheets accumulated under icehouse conditions suggests that in this global climate regime the cannibalization of eolian deposits was more common, in accord with the preservation of relatively thinner eolian architectural elements (dune sets, sandsheets, interdunes). The preferential cannibalization of eolian systems under icehouse conditions indicates a propensity for these systems to develop a negative sediment budget (likely due to exhaustion of an upwind eolian sediment supply).

The greater propensity for icehouse eolian systems to experience post-depositional deflation is supported by the textural analysis of icehouse and greenhouse deposits. Overall, analysis of sediment textures reveals that icehouse deposits are less texturally mature, have higher mean values of modal grain sizes, are relatively more poorly sorted, and have grains that are significantly more angular. The reduced textural maturity of icehouse sediments may be attributed to the relatively coarse and angular nature of grains that constitute a winnowed lag left being during the development of sandsheet elements (Nielsen and Kocurek, 1986; Pye and Tsoar, 1990; Mountney and Russell, 2004, 2006). However, the differences in grain size and sorting are not sufficiently large to be considered statistically significant; this finding is congruous with the highly discriminant nature of sediment transport by wind (Bagnold, 1941), which may generate a relatively well-sorted sediment source prior to deflation.

Greenhouse Conditions

The fact that dune-set, sandsheet and interdune architectural elements are significantly thicker in successions accumulated under greenhouse conditions, relative to those relating to icehouse conditions (Fig. 4) is attributed to their greater preservation potential over 100-400 kyr timescales. Relative to icehouse conditions, greenhouse Earth provides favorable conditions for the rapid incorporation of eolian elements into the geological record. Greenhouse conditions are associated with high eustatic levels and more-humid conditions, which generally promote elevated water tables situated close to the accumulation surface (Kocurek et al., 2001; Cowling, 2016).

Although the greenhouse geological record testifies to temporal variations in humidity (e.g., Sames et al., 2020), the greenhouse Earth did not generally experience large-magnitude shifts in global climate, relative to the glacial-interglacial oscillations of icehouse periods. As such, greenhouse conditions are generally associated with consistently elevated water tables, which experience only minor temporal changes in elevation relative to the accumulation surface (Fig. 11). Consistently elevated water tables can effectively sequester eolian successions; accumulating eolian successions are rapidly buried beneath the level of the water table, in response to progressive but gradual subsidence, and are accordingly protected from potential deflation by the wind, leading to the long-term accumulation of eolian systems (Fig. 11; Kocurek and Havholm, 1993; Mountney and Russell, 2009). Elevated water-table conditions are supported by the greater proportion of ‘wet’ interdune and ‘sabkha’ elements in greenhouse eolian successions (Evans, et al., 1964; Purser and Evans, 1973; Fryberger et al., 1990; Kocurek and Havholm, 1993; Garcia-Hidlago, 2002).

Elevated water tables interact with the accumulation surface to generate damp and wet substrates that inhibit the deflation of eolian sand deposits; greater threshold velocities are required to entrain wet or damp sand due to capillary water tension (Chepil, 1956; Bisal and Hsieh, 1966; Azizov, 1977). Humid, shallow water-table conditions may also promote the colonization of eolian substrates by vegetation or biogenic films or crusts in some paleoenvironmental settings (Basilici et al., 2020). Vegetation can limit the mobility of channelized river systems, which can potentially erode contiguous adjacent eolian deposits (Davies and Gibling, 2010; Reis et al., 2020; Santos et al., 2017, 2020). Moreover, vegetation can play a crucial role in dune construction and stabilization; vegetation disrupts primary airflows in the near-surface layer, decelerating winds and leading to the fall-out from the airflow of airborne sand grains (Kocurek and Nielsen, 1986), thereby promoting deposition; once deposited, vegetation can effectively trap eolian sediment, protecting it from re-suspension and potential erosion (Byrne and McCann, 1990; Ruz and Allard, 1994). The precipitation of early diagenetic cements around plant-root structures in eolian sand can further stabilize eolian surfaces (Mountney 2006).

The role of vegetation is only relevant for icehouse and greenhouse systems deposited after ca. 420 Ma, when vascular land plants became widespread (Gifford and Foster, 1989; Rainbird, 1992; Long, 2006; Davies and Gibling, 2010). However, the statistically significant difference in mean eolian architectural element thickness for icehouse and greenhouse conditions is also present in pre-vegetation Precambrian settings (see section ***'Precambrian Supercontinent')***. It can therefore be inferred that vegetation may play a contributing, but not crucial, role in determining eolian element thickness. Prior to the evolution of land plants, other biotic stabilizing agents likely played a role in limiting eolian winnowing, notably the presence of microbial films and crusts (e.g., Basilici et al., 2020).

The inference of the role played by stabilizing agents and higher water tables in minimizing eolian deflation is supported by the nature of supersurfaces seen in greenhouse systems, which are less likely to be deflationary than those formed under icehouse conditions (Fig. 7A). Greenhouse supersurfaces may be more likely to develop due to changes in depositional environment, such as fluvial inundation (Fig. 11), or the development of sabkha elements. The close proximity of the water table to the surface is interpreted to result in more closely spaced supersurfaces in greenhouse eolian successions.

Non-Eolian Elements

Non-eolian elements, which interdigitate with eolian elements to varying degrees, and which form over a third of all recorded element types by number of occurrences (comprising 37% and 38% of icehouse and greenhouse successions, respectively) in otherwise eolian-dominated successions, do not show a statistically significant difference in mean thickness between icehouse and greenhouse conditions. This might indicate that, within dominantly eolian systems, the thicknesses of interdigitated non-eolian elements are not primarily controlled by factors that are inherent to icehouse and greenhouse climatic conditions. This supports the idea that variations in eolian element thicknesses noted between icehouse and greenhouse systems are largely due to the effects of changes in wind strength as a driver of eolian accumulation and deflation. Many non-eolian elements are associated, to varying degrees, with deposition in aqueous environments and are therefore unaffected or slightly affected by changes in wind speed, strength and erosive power.

Other Boundary Conditions

Supercontinental Setting

The paleogeographic configuration and distribution of land masses has influenced sea level, global temperatures and patterns of atmospheric circulation. Only two paleogeographic states have existed in Earth history than spanned both icehouse and greenhouse conditions: the Precambrian and Pangean supercontinental configurations. When icehouse and greenhouse conditions are separately compared for these two supercontinental settings, the same statistical differences in eolian element thicknesses persist, such that eolian deposits associated with icehouse conditions are significantly thinner than those associated with greenhouse conditions. This suggests that the prevailing global climate regime may have influenced the development and preservation of eolian systems across different supercontinental configurations. The Precambrian and Pangean supercontinents are considered below.

Precambrian Supercontinents Evidence of Precambrian glaciogenic deposits have been recorded from many continental land masses, including those originally placed at tropical paleolatitudes (Shrag, 2002; Kirschvink, 1992). Precambrian icehouse conditions are attributed to attenuated solar luminosity, the albedo caused by continental landmasses located at low-latitudes, and relatively low levels of atmospheric carbon dioxide (Hoffman et al., 1998; Kirschvink, 1992).

In rocks of Precambrian age, icehouse eolian deposits are significantly thinner relative to their greenhouse counterparts (Fig. 8A). Changes in the strength and erosive power of the trade winds are likely equally relevant for eolian deposits of Precambrian age, as Hadley cell circulation is shown to have been active since the Proterozoic (Hoffman and Grotzinger, 1993). As such, the greater strength and erosive power of icehouse winds (Fig. 2) may be responsible for enhanced winnowing and deflation of Precambrian icehouse eolian architectural elements. Precambrian icehouse conditions are considered to have been amongst the most extreme of all recorded icehouse periods; wind strength and erosive power are interpreted to have been amongst the highest in Earth history (Fig. 2; Kirschvink, 1992; Allen and Hoffman, 2005).

Several of the studied Precambrian successions are associated with deposition in intracratonic basins, which are preferentially developed in the interiors of stable ancient cratons (e.g., Shaw et al., 1991; Aspler and Chiarenzelli, 1997; Deb and Pal, 2015), and which act as sites where relatively thin eolian elements can accumulate and be preserved, through episodic deposition between long periods of sediment bypass, controlled in part by relatively slow rates of subsidence and accommodation generation (e.g., Bethke, 1985; Aspler and Chiarenzelli, 1997). However, the differences in eolian element thickness between icehouse and greenhouse successions cannot be ascribed to the basin setting that hosts them (Fig. 12). In this study, greenhouse Precambrian deposits are all associated with accumulation in intracratonic basins, however, their icehouse counterparts are largely associated with deposition in continental rift and peripheral foreland basin settings; Fig. 12). Even though a bias in this study exists whereby the studied Precambrian greenhouse eolian deposits were all deposited in slowly subsiding intracratonic basins, the elements that make up these deposits are still significantly thicker than their Precambrian icehouse counterparts (Fig. 8A). This suggests that the climatic influence on eolian element thickness overrides the potential control on preservation of accommodation generation and basin morphology.

Pangean Supercontinent The Late Paleozoic is associated with a transition from icehouse to greenhouse conditions and changes in global atmospheric circulation (e.g., Rowley et al., 1985; Cecil, 1990; Parrish, 1993; West et al., 1997; Gibbs et al., 2002). The Late Paleozoic global climate change was closely associated with the formation of the Pangean supercontinent. The assemblage of Pangea resulted in the aggregation of large volumes of continental landmasses centered on the South Pole (Smith et al., 1973; McElhinny et al., 1981; Ziegler et al., 1983), which experienced widespread continental glaciation from ca.

360 to 300 Ma. The spread of continental glaciation was halted by increasing levels of atmospheric carbon dioxide and the northward drift of the continents: after ca. 300 Ma, the Earth tipped back into greenhouse climatic conditions (Parrish, 1993). The Pangean supercontinent disrupted zonal atmospheric circulation, leading to the development of the Pangean megamonsoon, which is comparable to the East Asian Monsoon and was characterized by a seasonal reversal of winds (Kutzbach and Gallimore, 1989; Parrish, 1993). The megamonsoon was active in the Permian, intensified into the Triassic, and continued on the Gondwanan supercontinent until the beginning of the Cretaceous (Parrish, 1993; Scherer and Goldberg, 2007; Scherer et al., 2020).

The megamonsoon and its associated seasonal reversals in wind direction are widely documented in the eolian record and have likely influenced the architecture of eolian deposits (e.g., Loope et al., 2001). It can thus be hypothesized that the megamonsoon may have also governed accumulated eolian element thickness, perhaps in a way that would have overprinted the effects of the controls exerted by icehouse and greenhouse conditions. However, despite the additional control imposed by megamonsoon conditions, icehouse eolian architectural elements (i.e. dune-sets, sandsheets and interdunes) remain significantly thinner than greenhouse architectural elements in stratigraphies of this age (Fig. 8A). Moreover, the mean thickness of greenhouse Pangean architectural elements (i.e. those deposited under peak megamonsoon conditions) does not differ significantly from greenhouse architectural elements deposited under comparable supercontinental settings (Fig. 13; Table 3). The impact of the megamonsoon on accumulated eolian element thickness is therefore considered to have been secondary compared to the climatic influence of icehouse-greenhouse oscillations. However, a limitation exists in this analysis, since icehouse conditions only prevailed on Pangea during its initial accretion, and the Pangean climate was dominated by greenhouse conditions for the majority of its existence.

Basin Configuration

The long-term preservation of eolian systems in the geological record requires the development of accommodation in which eolian deposits can accumulate. The basin morphology and rate of accommodation generation varies significantly between the basin types considered here (intracratonic, rift and foreland basins; see Table 2). Despite this, statistical differences between the thicknesses of icehouse and greenhouse architectural elements are noted for all basin types considered in this study (Fig. 8B), whereby eolian architectural elements associated with icehouse periods are significantly thinner than those of greenhouse periods. This suggests that the climatic influence on eolian element thickness overrides the potential controls of accommodation generation and basin morphology.

Paleolatitude

The preserved architecture of eolian systems is influenced by the latitude at which the eolian systems developed (Fig. 8C). The existence of the icehouse/greenhouse signature at low latitudes (<30°), and the absence of this signature at higher latitudes (>30°), supports the previous assertion that the differences in eolian element thicknesses are governed by atmospheric circulation at low latitudes, caused by icehouse/greenhouse modulation of the Hadley circulation, and associated with changes in the strength of the trade winds (Chandler, 1992; Lu et al., 2007; Hasegawa et al., 2011). Outside the zone of influence of the trade winds (>30° latitude), the icehouse-greenhouse signature is apparently not evident in the geological record; this suggests that the effects of global climate oscillations are overprinted by other forcing mechanisms in that context, such as rate and type of sediment supply, tectonic configuration, basin setting and dune-field physiographic setting.

Dune-field (Erg) Physiographic Setting

Across the different dune-field settings of eolian sand seas (i.e. back, center and fore erg-settings), variations in eolian element thickness are seen, with central-erg eolian architectural-elements being on average thicker than fore- and back-erg elements. However, across all environments of eolian sand seas, statistically significant differences in eolian architectural element thickness are seen between icehouse and greenhouse successions, such that icehouse eolian elements are consistently thinner relative to greenhouse architectural elements (Fig. 8D). The fact that this difference is seen across all dune-field physiographic settings corroborates the idea that the differences in eolian element thickness are the result of large-scale circulation patterns, which overprint signatures associated with localized and autogenic controls.

CONCLUSIONS

The continental terrestrial record has here been shown to preserve a valuable archive of how ancient sedimentary systems respond to and record changes in global climate. This study provides the first integrated global-scale quantitative investigation into the effects of climatic oscillations on eolian sedimentary architecture. More than >5,600 geological entities extracted from 34 case studies, spanning a variety of spatio-temporal settings, have been analyzed (Fig. 1). Icehouse and greenhouse conditions exert a fundamental and statistically detectable influence on preserved eolian dune-set, sandsheet and interdune thicknesses (Fig. 4; Table 3), such that icehouse eolian architectural elements are significantly thinner than greenhouse architectural elements. This statistical signature is present regardless of (i) basin type, (ii) paleogeographic configuration, and (iii) dune-field (erg) physiographic setting (Fig. 8; Table 3). However, the icehouse-greenhouse signature is only present at paleolatitudes <30°; it is absent in systems from higher paleolatitudes (Fig. 8C). Differences in eolian element thicknesses are interpreted in terms of changes in the pattern of circulation of low-latitude trade winds (Fig. 2), which operate at latitudes <30°.

Under icehouse conditions, Milankovitch-driven cycles of eolian accumulation and deflation result in the preservation of thin eolian architectural elements (i.e. dune sets, sandsheets and interdunes Figs. 4, 10); as an icehouse glacial initiates, thin dune sets and sandsheets are deposited under high wind strengths. As the glacial proceeds, higher trade-wind strengths result in the deposition of relatively thicker dune-sets, until upwind sources are exhausted (Fig. 10). The thick glacial dune-sets have limited preservation potential due to depressed water tables and the highly erosive nature of the strengthened trade winds. During interglacial periods, relative rises in the water-table enable the preservation of the thin basal dune-sets and sandsheets (Fig. 10).

Relative to greenhouse conditions, icehouse conditions are also associated with (i) a greater proportion of deflation-lag facies in sandsheet and interdune elements; (ii) relatively more observations of sandsheet strata, indicative of higher wind strengths; and (iii) a higher proportion of deflationary supersurfaces (Fig. 7). Consistently and significantly thicker greenhouse deposits are attributed to relatively elevated water tables (associated with wet interdunes and sabkha elements), which exhibit only minor temporal variations in level relative to the accumulation surface, and enhanced surface stabilization by vegetation or other biotic agents, all of which inhibit eolian deflation. Relative to icehouse conditions, greenhouse conditions are associated with: (i) eolian architectures dominated by an increased occurrence of dune-set elements, with fewer recorded sandsheet and interdune elements (Fig. 3B); (ii) interdunes that, where present, are more likely to be of a damp or wet type (Fig. 5A); (iii) a greater proportion of interdigitating sabkha elements (Fig. 3C).

This study presents a quantitative assessment of how the influence of icehouse and greenhouse climates on Earth surface processes is archived in the continental stratigraphic record. The results presented here provide novel insights into the fundamental boundary conditions that govern eolian sedimentary architectures, and have been used to develop idealized eolian icehouse and greenhouse facies models based on the most likely association of eolian and associated non-eolian architectural elements and bounding surfaces. The architectures of low-latitude eolian systems are fundamentally influenced by the prevailing global climate, and the way this influence has been translated into the stratigraphic record has been consistent through geological time. Results presented here help quantify and understand sedimentary responses to fundamental processes that operate on the surface of the Earth as a consequence of changes in global climate. In the context of human-induced climate change, these findings may be valuable for future predictions of the response of the terrestrial geosphere to fundamental changes in global climate.

AKNOWLEDGMENTS

We thank reviewers E. Simpson, an anonymous reviewer and the Associate Editor and Editor of GSA Bulletin for their constructive comments, which improved the paper. We thank the sponsors and partners of FRG-ERG for financial support for this research: AkerBP, Areva (now Orano), BHPBilliton, Cairn India (Vedanta), ConocoPhillips, Chevron, Equinor, Murphy Oil, CNOOC, Occidental, Petrotechnical Data Systems, Saudi Aramco, Shell, Tullow Oil, Woodside and YPF.

REFERENCES

Ager, D.V., 1993, The Nature of the Stratigraphical Record, 3rd edn. John Wiley & Sons, Chichester, New York, Brisbane, Toronto, Singapore, 151 pp.

Ahlbrandt, T.S., Andrews, S. and Gwynne, D.T., 1978, Bioturbation in eolian deposits, Journal of Sedimentary Petrology, v. 48, p. 839–848.
doi.org/10.1306/212F7586-2B24-11D7-8648000102C1865D

Allen, J.R.L., 1963, The classification of cross-stratified units with notes on their origin, Sedimentology, v. 2, p. 93–114.
doi.org/10.1111/j.1365-3091.1963.tb01204.x

Andrew, R. M., A comparison of estimates of global carbon dioxide emissions from fossil carbon sources, Earth System Science Data, v. 12, p. 1437–1465,
doi.org/10.5194/essd-12-1437-2020, 2020.

Andreucci, S., Clemmensen, L.B. and Pascucci, V., 2010, Transgressive dune formation along a cliffed coast at 75ka in Sardinia, Western Mediterranean: a record of sea-level fall and increased windiness. Terra Nova, v. 22, p. 424–433.
doi.org/10.1111/j.1365-3121.2010.00971.x

Anton, D., 1983, Modern eolian deposits of the eastern province of Saudi Arabia, in Brookfield, M.E. and Ahlbrandt, T.S., Eolian Sediments and Processes, Developments in Sedimentology, v. 38, p. 365-378.
doi.org/10.1016/S0070-4571(08)70805-7

Aspler, L.B. and Chiarenzelli, J.R., 1997, Initiation of 2.45–2.1 Ga intracratonic basin sedimentation of the Hurwitz Group, Keewatin Hinterland, Northwest Territories, Canada, Precambrian Research, v. 81, p. 265-297.

doi.org/10.1016/S0301-9268(96)00038-1

Atchley, S.C. and Loope, D.B., 1993, Low-stand aeolian influence on stratigraphic completeness: upper member of the Hermosa Formation (latest Carboniferous), southeast Utah, USA. In Pye, K. and Lancaster, N., Aeolian Sediments: Ancient and Modern, 127 – 149 pp.
doi.org/10.1002/9781444303971.ch9

Azizov, A., 1977, Influence of soil moisture on the resistance of soil to wind erosion, Soviet Soil Science, v. 9, p. 105-108. ISSN: 0038-5832

Bagnold, R.A., 1941, The physics of blown sand and desert dunes, London: Methuen.

Bállico, M.B., Scherer, C.M.S., Mountney, N.P., Souza, E.G., Chemale, F., Pisarevsky, S.A. and Reis A.D., 2017, Wind-pattern circulation as a palaeogeographic indicator: Case study of the 1.5-1.6 Ga Mangabeira Formation, Sao Francisco Craton, Northeast Brazil, Precambrian Research, v. 298, p. 1-15.
doi.org/10.1016/j.precamres.2017.05.005

Bart, H.A., 1977, Sedimentology of cross-stratified sandstones in Arikaree Group, Miocene, Southeastern Wyoming, Sedimentary Geology, v. 19, p. 165-184.
doi.org/10.1016/0037-0738(77)90029-X

Basilici, G., Dal' Bo, P.F.F. and Ladeira, F.S.B., 2009, Climate-induced sediment-palaeosol cycles in a Late Cretaceous dry aeolian sand sheet: Marília Formation (North-West Bauru Basin, Brazil), Sedimentology, v. 56, p. 1876-1904.
doi.org/10.1111/j.1365-3091.2009.01061.x

Basilici, G., Vinicius, M., Soares, T., Mountney, N.P., Colombera, L., 2020, Microbial influence on the accumulation of Precambrian aeolian deposits (Neoproterozoic, Venkatpur Sandstone Formation, Southern India), Precambrian Research, v. 347, 105854.
doi.org/10.1016/j.precamres.2020.105854

Benan, C.A.A. and Kocurek, G., 2000, Catastrophic flooding of an aeolian dune field: Jurassic Entrada and Todilto Formations, Ghost Ranch, New Mexico, USA, Sedimentology, v. 47, p. 1069-1080.
doi.org/10.1046/j.1365-3091.2000.00341.x

Bethke, C.M., 1985, A numerical model of compaction-driven groundwater flow and heat transfer and its application to the paleohydrology of intracratonic sedimentary basins, Journal of Solid Earth, v. 90, p. 6817-6828.
doi.org/10.1029/JB090iB08p06817

Bisal, F. and Hsieh, J., 1966, Influence of moisture on erodibility of soil by wind, Soil Science, v. 102, p. 143-146.

Biswas, A., 2005, Coarse aeolianites: sand sheets and zibar-interzibar facies from the Mesoproterozoic Cuddapah Basin, India, Sedimentary Geology, v. 174, p. 149-160.
doi.org/10.1016/j.sedgeo.2004.11.005

Blakey, R.C., 1988, Basin tectonics and erg response, Sedimentary Geology, v. 56, p. 127-151. doi.org/10.1016/0037-0738(88)90051-6

Blakey, R.C. and Middleton, L.T., 1983, Permian shoreline eolian complex in central Arizona: dune changes in response to cyclic sea-level changes, in Brookfield, M.E and Ahlbrandt, T.S., eds., Eolian Sediments and Processes, Developments in Sedimentology, v.38, p. 551–581. Elsevier, Amsterdam.

doi.org/10.1016/S0070-4571(08)70813-6

Bowring, S., Myrow, P., Landing, E., Ramezani, J., and Grotzinger, J., 2003, Geochronological constraints on terminal Neoproterozoic events and the rise of Metazoans, Geophysical Research Abstracts, v. 5, 13,219. EGS - AGU - EUG Joint Assembly, Abstracts from the meeting held in Nice, France, 6 - 11 April 2003, abstract id. 13219

Breed, C.S. and Grow, T., 1979, Morphology and distribution of dunes in sand seas observed by remote sensing, in McKee, E.D., ed., A study of global sand seas, U.S. Government Printing Office, Washington, DC, pp 253–302.

Brenchley, P.J., Marshall, J. D., Carden, G.A.F., Robertson, D.B.R., Long, D.G.F., Meidla, T., Hints, L. and Anderson. T.F., 1994, Bathymetric and isotopic evidence for a short-lived Late Ordovician glaciation in a greenhouse period, Geology, v. 22, p. 295–29.
doi.org/10.1130/0091-7613(1994)022<0295:BAIEFA>2.3.CO;2

Bristow, C.S. and Mountney, N.P., 2013, Aeolian Landscapes, Aeolian Stratigraphy, in Shroder, J., ed., Treatise on Geomorphology, pp. 246-268. Elsevier, San Diegeo, USA

Brooke, B., 2001, The distribution of carbonate eolianite. Earth-Science Reviews, v. 55, p. 135–164.
doi.org/10.1016/S0012-8252(01)00054-X

Brookfield, M.E., 1977, The origin of bounding surfaces in ancient aeolian sandstones, Sedimentology, v. 24, p. 303-332.
doi.org/10.1111/j.1365-3091.1977.tb00126.x

Brookfield, M.E., 1992, Eolian systems, in Walker, R.G. and James, N.P., Facies Models. Response to Sea Level Change, Geological Association of Canada, pp. 143–156.

Byrne, M.-L. and McCann, S.B., 1989, Stratification models for vegetated coastal dunes in Atlantic Canada, Sedimentary Geology, v. 66, p. 165-179. doi.org/10.1016/0037-0738(90)90058-2

Cather, S.M., Connell, S.D., Chamberlin, R.M., McIntosh, W.C., Jones, G.E., Potochnik, A.R., Lucas, S.G. and Johnson, P.S., 2008, The Chuska erg: Paleogeomorphic and paleoclimatic implications of an Oligocene sand sea on the Colorado Plateau, Geological Society of America Bulletin, v. 120, p. 13-33. doi.org/10.1130/B26081.1.

Cecil, C.B., 1990, Paleoclimate controls on stratigraphic repetition of chemical and siliciclastic rocks, Geology, v. 18, p. 533–536. doi.org/10.1130/0091-7613(1990)018<0533:PCOSRO>2.3.CO;2

Chan, M.A. and Kocurek, G., 1988, Complexities in eolian and marine interactions: processes and eustatic controls on erg development, Sedimentary Geology, v. 56, p. 283-300. doi.org/10.1016/0037-0738(88)90057-7

Chandler, M.A., Rind, D. and Ruedy, R., 1992, Pangaean climate during the Early Jurassic: GCM simulations and the sedimentary record of paleoclimate, Geological Society of America Bulletin, v. 104, p. 543-559. doi.org/10.1130/0016-7606(1992)104<0543:PCDTEJ>2.3.CO;2

Chepil, W.S., 1956, Influence of moisture on erodibility of soil by wind, Soil Science Society of America Proceedings, v. 20, p. 288-292.

Chrintz, T. and Clemmensen, L.B., 1993, Draa reconstruction, the Permian Yellow Sands, northeast England, in Pye, K. and Lancaster, N., Aeolian sediments. Ancient and modern, International Association of Sedimentologists Special Publication, v. 16, p. 151-161.
doi.org/10.1002/9781444303971.ch10

Clarke, M.L. and Rendell, H.M., 1998, Climate change impacts on sand supply and the formation of desert sand dunes in the south-west U.S.A, Journal of Arid Environments, v. 39, p. 517–531.
doi.org/10.1006/jare.1997.0372

Clemens, S. C., 1998, Dust response to seasonal atmospheric forcing: Proxy evaluation and calibration, Paleoceanography, v. 13, p. 471–490.
doi.org/10.1029/98PA02131.

Clemmensen, L.B., 1985, Desert sand plain and sabkha deposits from the Bunter Sandstone formation (L.Triassic) at the northern margin of the German Basin, Geologische Rundschau, v. 74, p. 519-536.
doi.org/10.1007/BF01821209

Clemmensen, L.B., 1987, Complex star dunes and associated aeolian bedforms, Hopeman Sandstone (Permo-Triassic), Moray Firth Basin, Scotland, in Frostick, L.E. and Reid, I., Desert Sediments: Ancient and Modern, Geological Society of London Special Publictaion, 35, p. 213-231.
doi.org/10.1144/GSL.SP.1987.035.01.15

Clemmensen, L.B., 1988, Aeolian morphology preserved by lava cover, the Precambrian Mussartut Member, Eriksfjord Formation, South Greenland, Bulletin of the Geological Society of Denmark, v. 37, p. 105-116.

Clemmensen L.B., 1991, Controls on aeolian sand sheet formation exemplified by the Lower Triassic of Helgoland, in Barndorff-Nielsen O.E., Willetts B.B., eds, Aeolian Grain Transport. Acta Mechanica Supplementum, v. 2. Springer, Vienna. doi.org/10.1007/978-3-7091-6703-8_12

Clemmensen, L.B. and Abrahamsen, K., 1983, Aeolian stratification and facies association in desert sediments, Arran basin (Permian), Scotland, Sedimentology, v. 30, p. 311-339. doi.org/10.1111/j.1365-3091.1983.tb00676.x

Clemmensen, L.B. and Abrahansen, K., 1983, Aeolian stratification and facies association in desert sediments, Arran Basin (Permian), Scotland, Sedimentology, v. 30, p. 311-339. doi.org/10.1111/j.1365-3091.1983.tb00676.x

Clemmensen, L.B. and Blakey, R.C., 1989, Erg deposits in the Lower Jurassic Wingate Sandstone, Northeastern Arizona: Oblique dune sedimentation, Sedimentology, v. 36, p. 449-470. doi.org/10.1111/j.1365-3091.1989.tb00619.x.

Clemmensen, L.B., Fornós, J.J. and Rodríguez-Perea, A., 1997, Morphology and architecture of a late Pleistocene cliff-front dune, Mallorca, Western Mediterranean. Terra Nova, v. 9, p. 251–254. doi.org/10.1111/j.1365-3121.1997.tb00023.x

Cojan, I. and Thiry, M., 1992, Seismically induced deformation structures in Oligocene shallow-marine and aeolian coastal sands (Paris Basin), Tectonophysics, v. 206, p. 78-89. doi.org/10.1016/0040-1951(92)90369-H

Coleman, A.P., 1907, A lower Huronian ice age. American Journal of Science, v. 23, p. 187–192.

Colombera, L., Mountney, N.P. and McCaffrey, W.D., 2012, A relational database for the digitization of fluvial architecture concepts and example applications, Petroleum Geoscience, v. 18, p. 129-140. doi.org/10.1144/1354-079311-021

Colombera, L., Mountney, N.P., Hodgson, D.M. and McCaffrey, W.D., 2016, The Shallow-Marine Architecture Knowledge Store: A database for the characterization of shallow-marine and paralic depositional systems, Marine and Petroleum Geology, v. 75, p. 83-99. doi.org/10.1016/j.marpetgeo.2016.03.027

Cowan, G., 1993, Identification and significance of aeolian deposits within the dominantly fluvial Sherwood Sandstone group of the East Irish Sea Basin UK, in North, C.P. and Prosser, D.J., eds., Characterization of fluvial and aeolian reservoirs, Geological Society of London Special Publication, v. 73, p. 231-245. doi.org/10.1144/GSL.SP.1993.073.01.14

Cowling, S.A., 2016, Sea level and ground water table depth (WTD): A biogeochemical pacemaker for glacial-interglacial cycling, Quaternary Science Reviews, v. 151, p. 309-314. doi.org/10.1016/j.quascirev.2016.09.009

Crabaugh, M. and Kocurek, G., 1993, Entrada Sandstone: An example of a wet aeolian system, in Pye, K., ed., The dynamics and environmental context of aeolian sedimentary systems, Geological Society of London Special Publication, v. 72, p. 103-126. doi.org/10.1144/GSL.SP.1993.072.01.11

Crowell, J.C., 1999, Pre-Mesozoic Ice Ages: Their Bearing on Understanding the Climate System: Boulder, Colorado, Geological Society of America Memoir 192, p. 2-77. ISBN: 0813711924, 9780813711928

Dal' Bo, P.F.F., Basilici, G. and Angélica, R.S., 2010, Factors of paleosol formation in a Late Cretaceous eolian sand sheet paleoenvironment, Marília Formation, Southeastern Brazil, Palaeogeography, Palaeoclimatology and Palaeoecology, v. 292, p. 349-365. doi.org/10.1016/j.palaeo.2010.04.021

Dasgupta, P.K., Biswas, A. and Mukherjee, R., 2005, Cyclicity in Palaeoproterozoic to Neoproterozoic Cuddapah Supergroup and its significance in basinal evolution, in Mabesoone, J.M. and Neumann, V.H., Cyclic Development of Sedimentary Basins, Developments in Sedimentology, v. 57, p. 313-354. doi.org/10.1016/S0070-4571(05)80013-5

Davies, N.S. and Gibling, M.R., 2010, Cambrian to Devonian evolution of alluvial systems: The sedimentological impact of the earliest land plants, Earth Science Reviews, v. 98, p. 171-200. doi.org/10.1016/j.earscirev.2009.11.002

Deb, M. and Pal, T., 2015, Mineral potential of Proterozoic intracratonic basins in India, in: Mazumder, R. and Eriksson, P.G., eds., Precambrian Basins on India, Geological Society of London, Memoir, v. 43, p. 309-325.
doi.org/10.1144/M43.21

Dias, K.D.N. and Scherer, C.M.S., 2008, Cross-bedding set thickness and stratigraphic architecture of aeolian systems: An example from the Upper Permian Piramboia Formation (Parana Basin), southern Brazil, Journal of South American Earth Sciences, v. 25, p. 405-415. doi.org/10.1016/j.jsames.2007.07.008

Dickinson, W.R., Soreghan, G.S. and Giles, K.A., 1994, Glacio-eustatic origin of Permo-carboniferous stratigraphic cycles: evidence from the southern Cordilleran foreland region, in Dennison, J.M. and Ettensohn,

F.R., eds., Tectonic and Eustatic Controls on Sedimentary Cycles, Society for Sedimentary Geology Concepts in Sedimentology and Paleontology, v. 4, p. 25–34.
doi.org/10.2110/csp.94.04.0025

Dott, R.H., Byers, C.W., Fielder, G.W., Stenzel, S.R. and Winfree, K.E., 1986, Aeolian to marine transition in Cambro-Ordovician cratonic sheet sandstones of the northern Mississippi valley, U.S.A, Sedimentology, v. 33, p. 345-367.
doi.org/10.1111/j.1365-3091.1986.tb00541.x

Dott, Jr., R., 2003, The Importance of Eolian Abrasion in Supermature Quartz Sandstones and the Paradox of Weathering on Vegetation-Free Landscapes. The Journal of Geology, v. 111, p. 387-405. doi:10.1086/375286

Einsele, G., 2013, Sedimentary Basins: Evolution, Facies and Sediment Budgets, Springer, New York, NY, p. 4.
ISBN 978-3-662-04029-4

Ellis, D., 1993, The Rough Gas Field: distribution of Permian aeolian and non-aeolian reservoir facies and their impact on field development, Geological Society of London Special Publication 73, p. 265-277.
doi.org/10.1144/GSL.SP.1993.073.01.16

Eriksson, K.A., McClung, W.S. and Simpson, E.L., 2019, Sequence stratigraphic expression of greenhouse, transitional and icehouse conditions in siliciclastic successions: Paleozoic examples from the central appalachian basin, USA, Earth Science Reviews, v. 188, p. 176 – 189.

doi.org/10.1016/j.earscirev.2018.11.010

Eriksson, P.G., Simpson, E.L., Eriksson, K.A., Bumby, A.J., Steyn, G.L. and Sarkar, S., 2000, Muddy Roll-up Structures in Siliciclastic Interdune Beds of the c. 1.8 Ga Waterberg Group, South Africa. PALAIOS, v. 15, p. 177–183.
doi: https://doi.org/10.1669/0883-1351(2000)015<0177:MRUSIS>2.0.CO;2

Evans, G., Kendall., C.G.St.C. and Skipwith, P., 1964, Origin of coastal flats, the sabkha of the Trucial Coast, Persian Gulf, Nature, v. 202, p. 759-761.
doi.org/10.1038/202759a0

Evans, D.A., Beukes, N.J., Kirschvink, J.L., 1997, Low-latitude glaciation in the Paleoproterozoic era, Nature v. 386, p. 262–266.
doi.org/10.1038/386262a0.

Folk, R.L. and Ward, W.C., 1957, Brazos River bar: a study in the significance of grain size parameters, Journal of Sedimentary Petrology, v. 27, p. 3–26.

Formolo Ferronatto, J.P., dos Santos Scherer, C.M., de Souza, E.G, dos Reis, A.D. and de Mello, R.G., 2019, Genetic units and facies architecture of a Lower Cretaceous fluvial-aeolian succession, Sao Sebastiao Formation, Jatoba Basin, Brazil, Journal of South American Earth Sciences, v. 89, p. 158-172.
doi.org/10.1016/j.jsames.2018.11.009

Fornós, J., Clemmensen, L.B., Gómez-Pujol, L. and Murray, A.S., 2009, Late Pleistocene carbonate aeolianites onMallorca, Western Mediterranean: a luminescencechronology. Quaternary Science Reviews, v. 28, p. 2697–2709.

doi.org/10.1016/j.quascirev.2009.06.008

Forster A., Schouten S., Baas M. and Sinninghe Damsté J. S., 2007, Mid-Cretaceous (Albian-Santonian) sea surface temperature record of the tropical Atlantic Ocean, Geology, v. 35, p. 919–922. doi.org.10.1130/G23874A.1

Frakes, L.A., Francis, J.E., and Syktus, J.I., 1992, Climate modes of the Phanerozoic, New York: Cambridge University Press, pp. 274.

Fryberger, S.G., 1993, A review of aeolian bounding surfaces, with examples from the Permian Minnelusa Formation, USA, in North, C.P. and Prosser, D.J., eds., Characterization of fluvial and aeolian reservoirs, Geological Society of London Special Publication 73, p.167-197. doi.org/10.1144/GSL.SP.1993.073.01.11.

Fryberger, S.G. and Schenk, C.J., 1988, Pin stripe lamination- a distinctive feature of modern and ancient eolian sediments, Sedimentary Geology, v. 55, p. 1-15. doi.org/10.1016/0037-0738(88)90087-5

Fryberger, S.G., Schenk, C.J. and Krystinik, L.F., 1988, Stokes surfaces and the effects of near-surface groundwater-table on Aeolian deposition, Sedimentology, v. 35, p. 21-41. doi.org/10.1111/j.1365-3091.1988.tb00903.x

Fryberger, S.G., Krystinik, L.F. and Schenk, C.J., 1990, Tidally flooded back-barrier dunefield, Guerrero Negro area, Baja California, Mexico, Sedimentology, v. 37, p. 23-43. doi.org/10.1111/j.1365-3091.1990.tb01981.x

García-Hidalgo, J.F., Temiño, J. and Segura, M., 2002, Holocene eolian sediments on the southern border of the Duero Basin (Spain): origin and development of an eolian system in a temperate zone, Journal of Sedimentary Research, v. 72, p. 30-39. doi.org/10.1306/040501720030

Gibbs, M.T., Rees, P.M., Kutzbach, J.E., Ziegler, A.M., Behling, P.J. and Rowley, D.B., 2002, Simulations of Permian climate and comparisons with climate-sensitive sediments, The Journal of Geology, v. 110, p. 33–55.
doi.org/10.1086/324204

Glennie, K.W. and Buller, A.T., 1983, The Permian Weissliegend of North West Europe. The partial deformation of aeolian dune sands caused by the Zechstein transgression, Sedimentary Geology, v. 35, p. 43-81.
doi.org/10.1016/0037-0738(83)90069-6

Goddéris, Y., Donnadieu, Y., Carretier, S., Aretz, M., Dera, G., Macouin, M. and Regard, V., 2017, Onset and ending of the late Palaeozoic ice age triggered by tectonically paced rock weathering, Nature Geoscience, v. 10, p. 382–386.
doi.org/10.1038/ngeo2931.

Guern, P.L. and Davaud, E., 2005, Recognition of ancient carbonate wind deposits: lessons from a modern analogue, Chrissi Island, Crete. Sedimentology, v. 52, p. 915–926.
doi.org/10.1111/j.1365-3091.2005.00700.x

Hasegawa, H., Tada, R., Jiang, X., Suganuma, Y., Imsamut, S., Charusiri, P., Ichinnorov, N. and Khand, Y., 2012, Drastic shrinking of the Hadley circulation during the mid-Cretaceous Supergreenhouse, Climate of the Past, v. 8, p. 1323-1337.
doi.org/10.5194/cp-8-1323-2012.

Hodgson, D.M., Bernhardt, A., Clare, M.A., Da Silva, A-C., Fosdick Julie, C., Mauz, B., Midtkandal, I., Owen, A., Romans, B.W., 2018, Grand Challenges (and Great Opportunities) in Sedimentology, Stratigraphy, and Diagenesis Research, Frontiers in Earth Science, v. 6, p. 173 Doi.org/10.3389/feart.2018.00173

Hoffman, P.F. and Grotzinger, 1993, Orographic precipitation, erosional unloading, and tectonic style, Geology, v. 21, p. 195-198. doi.org/10.1130/0091-7613(1993)021<0195:OPEUAT>2.3.CO;2

Hoffmann, K.-H., Condon, D.J., Bowring, S.A., and Crowley, J.L., 2004, U-Pb zircon date from the Neoproterozoic Ghaub Formation, Namibia: Constraints on Marinoan glaciation, Geology, v. 32, p. 817–820. doi.org/10.1130/G20519.1

Howell, J.A. and Mountney, N.P., 2001, Aeolian grain flow architecture: hard data for reservoir models and implications for red bed sequence stratigraphy, Petroleum Geoscience, v. 7, p. 51-56. doi.org/10.1144/petgeo.7.1.51

Hovan, S. A., and Rea, D.K., 1992, Paleocene Eocene boundary changes in atmospheric and oceanic circulation: A Southern Hemisphere record, Geology, v. 20, p. 15–18. doi.org/10.1130/00917613(1992)020<0015:PEBCIA>2.3.CO;2

Hovan, S.A., Rea, D.K., Pisias, N.G., 1991, Late Pleistocene Continental Climate and Oceanic Variability Recorded in Northwest Pacific Sediments, Paleoceanography and Paleoclimatology, v.6, p. 295-394. doi.org/10.1029/91PA00559

Hummel, G. and Kocurek, G., 1984, Interdune areas of the Back-Island dune field, North Padre-Island, Texas, Sedimentary Geology, v. 39, p. 1-26.

doi.org/10.1016/0037-0738(84)90022-8

Hunter, R.E., 1977, Basic types of stratification in small eolian dunes, Sedimentology, v. 24, p. 361–387. doi.org/10.1111/j.1365-3091.1977.tb00128.x

Hunter, R.E., 1981, Stratification styles in eolian sandstones: Some Pennsylvanian to Jurassic examples from the western interior USA, in Ethridge, F.G. and Flore, R.M., eds., Recent and Ancient Non-Marine Depositional Environments, Models for Exploration, Society for Sedimentary Geology Special Publication, v. 31, p. 315-329.
doi.org/10.2110/pec.81.31.0315

IPCC, 2007, Climate Change 2007: The Physical Science Basis, in Solomon, S., Qin, D., Manning, M., Chen, Z., Marquis, M., Averyt, K.B., Tignor, M., and Miller, H.L., eds., Contribution of Working Group I to the Fourth Assessment Report of the Intergovernmental Panel on Climate Change: Cambridge, Cambridge University Press, 996 p.

Irmen, A.P. and Vondra, C.F., 2000, Aeolian sediments in lower to middle (?) Triassic rocks of central Wyoming, Sedimentary Geology, v. 132, p. 69-88.
doi.org/10.1016/S0037-0738(99)00129-3

Jones, L.S. and Blakey, R.C., 1997, Eolian-fluvial interaction in the Page Sandstone (Middle Jurassic) in south-central Utah, USA: A case study of erg-margin processes, Sedimentary Geology, v. 109, p. 181-198.
doi.org/10.1016/S0037-0738(96)00044-9

Jones, F.H., dos Santos Scherer, C.M. and Kuchle, J., 2015, Facies architecture and stratigraphic evolution of aeolain dune and interdune deposits, Permian Caldeirao Member (Santa Brigida Formation), Brazil, Sedimentary Geology, v. 337, p. 133-150.

doi.org/10.1016/j.sedgeo.2016.03.018

Jordan, O.D. and Mountney, N.P., 2010, Styles of interaction between aeolian, fluvial and shallow marine environments in the Pennsylvanian to Permian lower Cutler beds, south-east Utah, USA, Sedimentology, v. 57, p. 1357-1385.
doi.org/10.1111/j.1365-3091.2010.01148.x

Jordan, O.D. and Mountney, N.P., 2012, Sequence stratigraphic evolution and cyclicity of an ancient coastal desert system: the Pennsylvanian-Permian Lower Cutler Beds, Paradox Basin, Utah, U.S.A, Journal of Sedimentary Research, v. 82, p. 755–780.
doi.org/10.2110/jsr.2012.54

Kidder, D.L. and Worsley, T.R., 2010, Phanerozoic Large Igneous Provinces (LIPs), HEATT (Haline Euxinic Acidic Thermal Transgression) episodes, and mass extinctions: Palaeogeography, Palaeoclimatology, Palaeoecology, v. 295, p. 162–191.
doi:10.1016/j.palaeo.2010.05.036.

Kidder, D.L. and Worsley, T.R., A human-induced hothouse climate? The Geological Society of America, v. 22, p. 4-11.
doi.org/10.1130/G131A.1.

Knoll, A.H., and Walter, M.R., 1992. Latest Proterozoic stratigraphy and Earth history, Nature, v. 356, p. 673–677.
doi.org/10.1038/356673a0

Kocurek, G., 1991, Interpretation of ancient eolian sand dunes, Annual Review of Earth and Planetary Science, v. 19, p. 43-75.

doi.org/10.1146/annurev.ea.19.050191.000355.

Kocurek, G., 1996, Desert aeolian systems, in Reading, H.G., eds., Sedimentary environments: processes, facies and stratigraphy, pp. 125-153, 3rd edition, Oxford: Blackwell.

Kocurek G., 1999, The aeolian rock record (Yes, Virginia, it exists but it really is rather special to create one), in Goudie, A.S., Livingstone, I., Stokes, S., eds., Aeolian Environments Sediments and Landforms, pp. 239-259, John Wiley and Sons Ltd, Chichester.

Kocurek, G., 1998, Aeolian System Response to External Forcing Factors - A Sequence Stratigraphic View of the Saharan Region, in Alsharan, A.S., Glennie, K.W. and Whittle, G.L., eds., Quaternary Deserts and Climatic Change, pp. 327-338. Balkema, Rotterdam/Brookfield

Kocurek, G. and Day, M., 2018, What is preserved in the aeolian rock record? A Jurassic Entrada Sandstone case study at the Utah–Arizona border, Sedimentology, v. 65, p. 1301-1321. doi.org/10.1111/sed.12422

Kocurek, G. and Dott, R.H., 1981, Distinctions and uses of stratification types in the interpretation of eolian sand, Journal of Sedimentary Petrology, v. 51, p. 579-595. doi.org/10.1306/212F7CE3-2B24-11D7-8648000102C1865D

Kocurek, G. and Fielder, G., 1982, Adhesion structures, Journal of Sedimentary Petrology, v. 52, p. 1229-1241. doi.org/10.1306/212F8102-2B24-11D7-8648000102C1865D

Kocurek, G. and Havholm, K.G., 1993, Eolian sequence stratigraphy-a conceptual framework, in Weimer, P. and Posamentier, H., eds., Siliciclastic Sequence Stratigraphy, American Association of Petroleum Geologists Memoir, v. 58, p. 393-409.
doi.org/10.1306/M58581C16

Kocurek, G. and Lancaster, N., 1999, Aeolian system sediment state: theory and Mojave Desert Kelso dune field example, Sedimentology, v. 46, p. 505-515.
doi.org/10.1046/j.1365-3091.1999.00227.x

Kocurek, G., Lancaster, N., Carr, M. and Frank, A, 1999, Tertiary Tsondab Sandstone Formation: preliminary bedform reconstruction and comparison to modern Namib Sand Sea dunes, Journal of African Earth Sciences, v. 29, p. 629-642.
doi.org/10.1016/S0899-5362(99)00120-7

Kocurek, G., Townsley, M., Yeh, E., Havholm, K. and Sweet, M.L., 1992, Dune and dune-field development on Padre Island, Texas, with implications for interdune deposition and water-table controlled accumulation, Journal of Sedimentary Petrology, v. 62, p. 622-635.
doi.org/10.1306/D4267974-2B26-11D7-8648000102C1865D

Kocurek, G., Robinson, N.I. and Sharp, J.M.J., 2001, The response of the water table in coastal aeolian systems to changes in sea level, Sedimentary Geology, v. 139, p. 1-13.
doi.org/10.1016/S0037-0738(00)00137-8

Kohfeld, K. E. and Harrison, S.P., 2001, DIRTMAP: The geological record of dust, Earth Science Reviews, v. 54, p. 81–114.
doi.org/10.1016/S0012-8252(01)00042-3

Krapovickas, V., 2012, Deposits of the Santa Cruz Formation (late early Miocene): paleohydrologic and paleoclimatic significance, in Vizcaíno, S.F., Kay, R.F. and Bargo, M.S., eds., Early Miocene paleobiology in Patagonia: High-latitude paleocommunities of the Santa Cruz Formation, pp. 91–103, Cambridge, Cambridge University Press.

Krumbein, W.C., 1941, Measurement and geological significance of shape and roundness of sedimentary particles, Journal of Sedimentary Petrology, v. 11, p. 64-72.

Kutzbach, J.E. and R.G. Gallimore, 1989, Pangaean climates: Megamonsoons of the megacontinent, Journal of Geophysical Research, v. 94, p. 3341-3357.
doi.org/10.1029/JD094iD03p03341

Lancaster, N., 1989, The Namib Sand Sea: Dune forms, processes and sediments, Taylor and Francis, 1989 Rotterdam: Balkema, p. 180.
ISBN: 9061916976, 9789061916970

Lancaster, N., 1990, Palaeoclimatic evidence from sand seas, Palaeogeography, Palaeoclimalology, and Palaeoecology, v. 76, p. 279-90.
doi.org/10.1016/0031-0182(90)90116-O

Lancaster, N. and Teller, J.T., 1988, Interdune deposits of Namib Sand Sea, Sedimentary Geology, v. 55, p. 91-107.
doi.org/10.1016/0037-0738(88)90091-7

Lauretano, V., Littler, K., Polling, M., Zachos, J. C. and Lourens, L. J., 2015, Frequency, magnitude and character of hyperthermal events at the onset of the Early Eocene Climatic Optimum, Climate of the Past, v. 11, p. 1313–1324.

doi.org/10.5194/cp-11-1313-2015.

Leleu, S. and Hartley, A.J., 2018, Constraints on synrift intrabasinal horst development from alluvial fan and aeolian deposits (Triassic, Fundy Basin, Nova Scotia), in Ventra, D. and Clarke, L.E., Geology and Geomorphology of Alluvial and Fluvial Fans: Terrestrial and Planetary Perspectives, Geological Society of London Special Publication, v. 440, p. 79-101.
doi.org/10.1144/SP440.8

Liesa, C.L., Rodríguez-López, J.P., Ezquerro, L., Alfaro, P., Rodriguez-Pascua, M.A., Lafuente, P., Arlegui, L. and Simon J.L., 2016, Facies control on seismites in an alluvial-aeolian system: The Pliocene dunefield of the Teruel half-graben basin (eastern Spain), Sedimentary Geology, v. 344, p. 237-252.
doi.org/10.1016/j.sedgeo.2016.05.009

Link P.K., 2009, “Icehouse” (Cold) Climates, in Gornitz V., eds., Encyclopedia of Paleoclimatology and Ancient Environments. Encyclopedia of Earth Sciences Series. Springer, Dordrecht.
doi.org/10.1007/978-1-4020-4411-3_112

Long, D.G.F., 2006, Architecture of pre-vegetation sandy-braided perennial and Ephemeral River deposits in the Paleoproterozoic Athabasca Group, northern Saskatchewan, Canada as indicators of Precambrian fluvial style, Sedimentary Geology, v. 190, p. 71-95.
doi.org/10.1016/j.sedgeo.2006.05.006

Loope, D.B., 1985, Episodic deposition and preservation of eolian sands – a Late Paleozoic example from southeastern Utah, Geology, v. 13, p. 73– 76.
doi.org/10.1130/0091-7613(1985)13<73:EDAPOE>2.0.CO;2

Loope, D.B. and Rowe C.M., 2003, Long-lived pluvial episodes during deposition of the Navajo Sandstone, The Journal of Geology, v. 111, p. 223-232.
doi.org/10.1086/345843

Loope, D., Rowe, C. and Joeckel, R., 2001, Annual monsoon rains recorded by Jurassic dunes, Nature, v. 412, p. 64–66.
doi.org/10.1038/35083554

Loope, D.B., Swinehart, J.B. and Mason, J.P., 1995, Dune-dammed paleovalleys of the Nebraska Sand Hills-intrinsic versus climatic controls on the accumulation of lake and marsh sediments, The Geological Society of America Bulletin, v. 107, p. 396-406.
doi.org/10.1130/0016-7606(1995)107<0396:DDPOTN>2.3.CO;2

Lu, J., Vecchi, G. A., and Reichler, T., 2007, Expansion of the Hadley cell under global warming, Geophysical Research Letters, v. 34, L06805.
doi.org/10.1029/2006GL028443

Mainguet, M. and Chemin, M. C., 1983, Sand seas of the Sahara and Sahel: an explanation of their thickness and sand dune type by the sand budget principle, in Brookfield, M.E. and Ahlbrandt, T.S., eds., Eolian Sediments and Processes, Developments in Sedimentology, v. 38, p. 353-363.
doi.org/10.1016/S0070-4571(08)70804-5

McElhinny, M., Embleton, B.J.J., Ma, X.H. and Zhang, Z.K., 1981, Fragmentation of Asia in the Permian, Nature, v. 293, p. 212-216.
doi.org/10.1038/293212a0

Meadows, N.S. and Beach, A., 1993, Structural and climatic controls on facies distribution in a mixed fluvial and aeolian reservoir: the Triassic Sherwood Sandstone in the Irish Sea, in North, C.P. and Prosser, D.J., eds., Characterization of fluvial and aeolian reservoirs, Geological Society of London Special Publication, v. 73, p. 247-264.
doi.org/10.1144/GSL.SP.1993.073.01.15

Melton M.A., 1965, The geomorphic and paleoclimatic significance of alluvial deposits in southern Arizona, The Journal of Geology, v. 73, p. 1–38.
doi.org/10.1086/627044

Middleton, G.V. and Southard, J.B., 1984, Mechanics of Sediment Movement, Society for Sedimentary Geology Short Course, 3, 401 pp.

Milankovitch, M., 1941, Kanon der Erdbestrahlung und seine Andwendung auf das Eiszeiten-problem, Royal Serbian Academy, Belgrade.

Mitchum, R. M., 1977, Seismic stratigraphy and global changes of sea level, Part I: Glossary of terms used in seismic stratigraphy, in Payten, C. E., ed., Seismic stratigraphy--applications to hydrocarbon exploration American Association of Petroleum Geologists Memoir, v. 26, p. 53-62.
doi.org/10.1306/M26490C13

Montañez, I.P. and Poulsen, C.J., 2013, The Late Paleozoic Ice Age: An Evolving Paradigm, Annual Review of Earth and Planetary Science, v. 41, p. 629-656.
doi.org/10.1146/annurev.earth.031208.100118

Morley, C.K., 1995, Developments in the structural geology of rifts over the last decade and their impact on hydrocarbon exploration, in Lambiase, J.J., ed., Hydrocarbon Habitat in Rift Basins, Geological Society of London, Special Publication 80, p. 1–32. doi.org/10.1144/GSL.SP.1995.080.01.01

Mountney, N.P., 2006, Periodic accumulation and destruction of aeolian erg sequences: The Cedar Mesa Sandstone, White Canyon, southern Utah, Sedimentology, v. 53, p. 789-823. doi.org/10.1111/j.1365-3091.2009.01072.x

Mountney, N.P. and Howell, J., 2000, Aeolian architecture, bedform climbing and preservation space in the Cretaceous Etjo Formation, NW Nambia, Sedimentology, v. 47, p. 825-849. doi.org/10.1046/j.1365-3091.2000.00318.x

Mountney, N.P. and Jagger, A., 2004, Stratigraphic evolution of an aeolian erg margin system: the Permian Cedar Mesa Sandstone, SE Utah, USA, Sedimentology, v. 51, p. 713-743. doi.org/10.1111/j.1365-3091.2004.00646.x

Mountney, N.P. and Russell, A.J., 2006, Coastal aeolian dune development, Solheimasandur, southern Iceland, Sedimentary Geology, v. 192, p. 167-181. doi.org/10.1016/j.sedgeo.2006.04.004

Mountney, N.P. and Russell, A.J., 2009, Aeolian dune-field development in a water-table controlled system: Skiđeararsándur, Southern Iceland, Sedimentology, v. 56, p. 2107-2131. doi.org/10.1111/j.1365-3091.2009.01072.x

Mountney, N.P., Howell, J., Flint, S. and Jerram, D., 1999, Climate, sediment supply and tectonics as controls on the deposition and preservation of the aeolian-fluvial Etjo Sandstone Formation, Namibia, Journal of the Geological Society of London, v. 156, p. 771-777.
doi.org/10.1144/gsjgs.156.4.0771

Newell, A.J., 2001, Bounding surfaces in a mixed aeolian-fluvial system (Rotliegend, Wessex Basin, SW UK), Marine and Petroleum Geology, v. 18, p. 339-347.
doi.org/10.1016/S0264-8172(00)00066-0

Nielson J. and Kocurek G., 1986, Climbing zibars of the Algodones, Sedimentary Geology, v. 48, p. 1-15.
doi.org/10.1016/0037-0738(86)90078-3

Nielsen, K.A., Clemmensen, L.B. and Fornós, J.J., 2004, Middle Pleistocene magnetostratigraphy and susceptibility stratigraphy: data from a carbonate Aeolian system, Mallorca, Western Mediterranean. Quaternary Science Reviews, v. 23, p. 1733–1756.
doi.org/10.1016/j.quascirev.2004.02.006

Nichols, G.J., 2005, Sedimentary evolution of the lower Clair Group, Devonian, west of Shetland; climate and sediment supply controls on fluvial, aeolian and lacustrine deposition, in Doré, A.G. and Vining, B.A., eds., Petroleum Geology of Northwest Europe, Proceedings of the Conference, published by the Geological Society of London, v. 6, p. 957-967.
doi.org/10.1144/0060957

Nickling, W.G., McKenna Neuman, C. and Lancaster, N., 2002, Grainfall processes in the lee of transverse dunes, Silver Peak, Nevada, Sedimentology, v. 49, p. 191–209.
doi.org/10.1046/j.1365-3091.2002.00443.x

Olsen, H., Due, P.H. and Clemmensen, L.B., 1989, Morphology and genesis of asymmetric adhesion warts—a new adhesion surface structure, Sedimentary Geology, v. 61, p. 277-285. doi.org/10.1016/0037-0738(89)90062-6

Parrish, J.T., 1993, Climate of the supercontinent Pangea, The Journal of Geology, v. 101, p. 215–233. doi.org/10.1086/648217

Parrish, J.T. and Petersen, F., 1988, Wind directions predicted from global circulation models and wind directions determined from eolian sandstones of the western United States- A comparison, Sedimentary Geology, v. 56, p. 261-282. doi.org/10.1016/0037-0738(88)90056-5

Peters, G.P., Andrew, R.M., Canadell, J.G., Friedlingstein, P., Jackson, R.B., Korsbakken, J.I., Le Quéré, C. and Peregon, A., 2020, Carbon dioxide emissions continue to grow amidst slowly emerging climate policies, Nature Climate Change, v. 10, p. 3–6. doi.org/10.1038/s41558-019-0659-6

Peterson, F., 1988, Pennsylvanian to Jurassic eolian transportation systems in the western United States, in G. Kocurek, G., ed., Late Palaeozoic and Mesozoic Eolian Deposits of the Western Interior of the United States, Sedimentary Geology, v. 56, p. 207-260. doi.org/10.1016/0037-0738(88)90055-3

Petit, J.R., Jouzel, J., Raynaud, D., Barkov, N.I., Barnola, J.-M., Basile, I., Bender, M., Chappellaz, J., Davis, M., Delaygue, G., Delmotte, M., Kotlyakov, V.M., Legrand, M., Lipenkov, V.Y., Lorius, C., Pépin, L., Ritz, C., Saltzman, E., and Stievenard, M., 1999, Climate and atmospheric history of the past 420,000 years from the Vostok ice core, Antarctica, Nature, v. 399, p. 429–436. doi.org/10.1038/20859

Pike, J.D. and Sweet, D.E., 2018, Environmental drivers of cyclicity recorded in lower Permian eolian strata, Manitou Springs, western United States, Palaeogeography, Palaeoclimatology, Palaeoecology, v. 499, p. 1-12.
doi.org/10.1016/j.palaeo.2018.03.026

Plint, G., Nummedal, D., 2000, The falling stage systems tract: Recognition and importance in sequence stratigraphic analysis, Geological Society London Special Publications, v. 172, p. 1-17.
doi.org/10.1144/GSL.SP.2000.172.01.01.

Porter, M.L., 1986, Sedimentary record of erg migrations, Geology, v. 14, p. 497-500.
doi.org/10.1130/0091-7613(1986)14<497:SROEM>2.0.CO;2

Price, G., Valdes, P.J and Sellwood, B.W., 1998, A comparison of GCM simulated Cretaceous ‘greenhouse’ and ‘icehouse’ climates: implications for the sedimentary record, Palaeogeography, Palaeoclimatology, Palaeoecology, v. 142, p. 123–138. doi.org/10.1016/S0031-0182(98)00061-3

Pulvertaft, T.C.R., 1985, Eolian dune and wet interdune sedimentation in the Middle Proterozoic Dala Sandstone, Sweden, Sedimentary Geology, v. 44, p. 93-111.
doi.org/10.1016/0037-0738(85)90034-X

Purser, B.H. and Evans, G., 1973, Regional sedimentation along the Trucial Coast, Persian Gulf, in Purser, B.H., eds., Persian Gulf, p.211-231, Berlin, Springer.

Pye, K., 1983, Early Post-Depositional Modification of Aeolian Dune Sands, in Brookfield, M.E. and Ahlbrandt, T.S., eds., Developments in Sedimentology, v. 38, p. 197-221.
doi.org/10.1016/S0070-4571(08)70796-9.

Pye, K., 2009, Aeolian bed forms, in Pye, K. and Tsoar, H., Aeolian sand and sand dunes, Unwin Hyman Limited, London, p. 175-253.
ISBN : 978-3-540-85909-3

Pye, K. and Tsoar, H., 1990, Aeolian sand and sand dunes, Unwin Hyman Limited, London, pp. 396.
ISBN : 978-3-540-85909-3

Rainbird, R.H., 1992, Anatomy of a large-scale braid-plain quartzarenite from the Neoproterozoic Shaler Group, Victoria Island, Northwest Territories, Canada, Canadian Journal of Earth Science, v. 29, p. 2537-2550.
doi.org/10.1139/e92-201

Rea, D. K., 1994, The paleoclimatic record provided by eolian deposition in the deep sea: The geologic history of wind, Reviews of Geophysics, v. 32, p. 159–195.
doi.org/10.1029/93RG03257.

Rea, D.K., Janecek, T.R., 1981, Mass-accumulation rates of the non-authigenic inorganic crystalline (Eolian) component of deep-sea sediments from the western Mid-Pacific Mountains, Deep Sea Drilling Project Site 463, in Thiede, J., Vallier, T.L., et al., eds., Initial Reports of the Deep Sea Drilling Project (U.S. Govt. Printing Office), v. 62, p. 653-659.

Reis, A.D.d., Scherer, C.M.S., Amarante, F.B., Rossetti, M.M.M., Kifumbi, C., Souza, E.G., Formolo Ferronatto, J.P and Owen, A., 2020, Sedimentology of the proximal portion of a large-scale, Upper Jurassic fluvial-aeolian system in Paraná Basin, southwestern Gondwana. Journal of South American Earth Sciences, v. 95, 102248.
doi.org/10.1016/j.jsames.2019.102248

Rodríguez-López, J.P., Meléndez, N., de Boer, P.L. and Soria, A.R. , 2012, Controls on marine-erg margin cycle variability: aeolian-marine interaction in the Mid-Cretaceous Iberian Desert System, Spain, Sedimentology, v. 59, p. 466-501.
doi.org/10.1111/j.1365-3091.2011.01261.x

Rodríguez-López, J.P., Clemmensen, L.B., Lancaster, N., Mountney, N.P. and Veiga, G.D., 2014, Archean to Recent aeolian sand systems and their sedimentary record: Current understanding and future prospects, Sedimentology, v. 61, p. 1487-1534. doi.org/10.1111/sed.12123

Rosendahl, B.R., 1987, Architecture of continental rifts with special reference to East Africa, Annual Review of Earth and Planetary Sciences, v. 15, p. 445–503.
doi.org/10.1146/annurev.ea.15.050187.002305

Rowley, D.B., Raymond, A., Parrish, J.T., Lottes, A.L., Scotese, C.R. and Ziegler, A.M., 1985, Carboniferous paleogeographic, phytogeographic, and paleoclimatic reconstructions, International Journal of Coal Geology, v. 5, p. 7–42. doi.org/10.1016/0166-5162(85)90009-6

Rubin, D.M. and Hunter, R.E., 1982, Bedform climbing in theory and nature, Sedimentology, v. 29, p. 121–138.
doi.org/10.1111/j.1365-3091.1982.tb01714.x

Ruz, M.-H. and Allard, M., 1994, Coastal dune development in cold-climate environments, Physical Geography, v. 15, p. 372–380.
doi.org/10.1080/02723646.1994.10642523
Sadler, P.M., 1981, Sediment accumulation rates and the completeness of stratigraphic sections, The Journal of Geology, v. 89, p. 569–584.
doi.org/10.1086/628623

Sames, B., Wagreich, M., Conrad, C.P. and Iqbal, S., 2020, Aquifer-eustasy as the main driver of short-term sea-level fluctuations during Cretaceous hothouse climate phases, Geological Society of London Special Publications, 498, p. 9-38.
doi.org/10.1144/SP498-2019-105

Sarnthein, M., 1978, Sand deserts during glacial maximum and climatic optimum, Nature, v. 272, p. 43-46.
doi.org/10.1038/272043a0

Scherer, M.S., Lavina, E.L.C., Dias Filho, D.C., Oliveira, F.M., Bongiolo, D.E. and Aguiar, E.S., 2007, Stratigraphy and facies architecture of the fluvial-aeolian-lacustrine Sergi Formation (Upper Jurassic), Reconcavo Basin, Brazil, Sedimentary Geology, v. 194, p. 169-193.
doi.org/10.1016/j.sedgeo.2006.06.002

Scherer, C.M.S. and Goldberg, K., 2007, Palaeowind patterns during the latest Jurassic-earliest Cretaceous in Gondwana: Evidence from aeolian cross-strata of the Botucatu Formation, Brazil, Palaeogeography, Palaeoclimatology, Palaeoecology, v. 250, p. 89-100.
doi.org/10.1016/j.palaeo.2007.02.018.

Scherer, C.M.A. and Lavina, L.C., 2005, Sedimentary cycles and facies architecture of aeolian–fluvial strata of the Upper Jurassic Guara Formation, southern Brazil, Sedimentology, v. 52, p. 1323-1341.
doi.org/10.1111/j.1365-3091.2005.00746.x

Scherer, C.M.S., Mello, R.G., Ferronatto, J.P.F, Amarante, F.B., Reis, A.D., Souza, E.G., and Goldberg, K,, 2020, Changes in prevailing surface-palaeowinds of western Gondwana during Early Cretaceous, Cretaceous Research, v. 116, 104598

Schlische, R.W., 1993, Anatomy and evolution of the Triassic-Jurassic continental rift system, eastern North America, Tectonics, v. 12, p. 1026–1042.
doi.org/10.1029/93TC01062

Schokker, J. and Koster, E.A., 2004, Sedimentology and facies distribution of Pleistocene cold-climate aeolian and fluvial deposits in the Roer Valley graben (Southeastern Netherlands), Permafrost and Periglacial Processes, v. 15, p. 1-20.
doi.org/10.1002/ppp.477

Semeniuk, V. and Glassford D.K., 1988, Significance of aeolian limestone lenses in quartz sand formations: an interdigitation of coastal and continental facies, Perth Basin, southwestern, Australia, Sedimentary Geology, v. 57, p. 199-209.
doi.org/10.1016/0037-0738(88)90027-9

Shackleton, N.J., Crowhurst, S.J., Weedon, G., and Laskar, L., 1999, Astronomical calibration of Oligocene-Miocene time: Royal Society of London Philosophical Transactions, v. 357, p. 1909–1927.
doi.org/10.1098/rsta.1999.0407

Shaw, R.D., Etheridge, M.A. and Lambeck, K., 1991, Development of the Late Proterozoic to Mid-Paleozoic, intracratonic Amadeus Basin in central Australia: A key to understanding tectonic forces in plate interiors, Tectonics, v. 10, p. 688-721.
doi.org/10.1029/90TC02417

Simplicio, F. and Basilici, G., 2015, Unusual thick eolian sand sheet sedimentary succession: Paleoproterozoic Bandeirinha Formation, Minas Gerais, Brazilian Journal of Geology, v. 45, p. 3-11.
doi.org/10.1590/2317-4889201530133

Simpson, E.L., Eriksson, K.A. and Muller, W.U., 2012, 3.2 Ga eolian deposits from the Moodies Group, Barberton Greenstone Belt, South Africa: Implications for the origin of first-cycle quartz sandstones, Precambrian Research, v. 214-215, p. 185-191. doi.org/10.1016/j.precamres.2012.01.019

Simpson, E.L., Fernando, A., Pradip, B., Bumby, A.J., Eriksson, K.A., Eriksson, P.G., Martins-Neto, M.A., Middleton, L.T. and Rainbird, R., 2004, Sedimentary dynamics in Precambrian aeolianites. In Eriksson, P.G., Altermann, W., Nelson, D.R., Mueller, W. and Catuneanu, O., eds., The Precambrian Earth: Tempos and Events, Elsevier, Amsterdam, pp. 675-677.

Simpson, E.L., Heness, E., Bumby, A., Eriksson, P.G., Eriksson, K.A., Hilbert-Wolf, H.L., Linnevelt, S., Fitzgerald Malena, H., Modungwa, T. and Okafor, O.J., 2013, Evidence for 2.0Ga continental microbial mats in a paleodesert setting. Precambrian Research, v. 237, p. 36-50. doi.org/10.1016/j.precamres.2013.08.001.

Simpson, E.L., Hilbert-Wolf, H.L., Simpson, W.S., Tindall, S.E., Bernard, J.J., Jenesky, T.A. and Wizevich, M.C., 2008, The interaction of aeolian and fluvial processes during deposition of the Upper Cretaceous capping sandstone member, Wahweap Formation, Kaiparowits Basin, Utah, U.S.A. Palaeogeography, Palaeoclimatology, Palaeoecology, v. 270, p. 19-28. doi.org/10.1016/j.palaeo.2008.08.009.

Smith, A.G., Briden, J.C. and Drewry, G.E., 1973, Phanerozoic world maps, in Hughes, N.F., ed., Organisms and Continents through Time, Special Paper of the Paleontological Association 12, p. 1-42.

Sorby, H.C., 1859, On the structures produced by the currents present during the deposition of stratified rocks, The Geologist, v. 2, p. 137–147. doi.org/10.1017/S1359465600021122

Soreghan, G.S., Heavens, N.G., Hinnov, L.A., Aciego, S.M., Simpson, C., 2015, Reconstructing the Dust Cycle in Deep Time: the Case of the Late Paleozoic Icehouse, The Paleontological Society Papers, v. 21, p. 83-120.
doi.org/10.1017/S1089332600002977.

Soria, A.R., Liesa, C.L., Rodríguez-López, J.P., Meléndez, N., de Boer, P.L. and Meléndez, A., 2011, An Early Triassic evolving erg system (Iberian Chain, NE Spain): Palaeoclimate implications, Terra Nova, v. 23, p. 76-84.
doi.org/10.1111/j.1365-3121.2011.00986.x

Stancin, A.M., Gleason, J.D., Hovan, S.A., Rea, D.K., Owen, R.M., More, T.C. Jr., Hall, C.M. and Blum, J.D., 2008, Miocene to recent eolian dust record from the southwest Pacific Ocean at 40°S latitude, Palaeogeography, Palaeoclimatology, Palaeoecology, v. 261, p. 218–233.
doi.org/10.1016/j.palaeo.2007.12.015

Stewart, J.H., 2005, Eolian deposits in the Neoproterozoic Big Bear Group, San Bernardino Mountains, California, USA, Earth Science Reviews, v. 72, p. 47-62.
doi.org/10.1016/j.earscirev.2005.07.012

Strömbäck, A. and Howell, J.A., 2002, Predicting distribution of remobilized aeolian facies using sub-surface data: the Weissliegend of the UK Southern North Sea, Petroleum Geoscience, v. 8, p. 237–249.
doi.org/10.1144/petgeo.8.3.237

Stokes, W.L., 1968, Multiple parallel-truncation bedding planes – a feature of wind deposited sandstone formations, Journal of Sedimentary Petrology, v. 38, p. 510–515.
doi.org/10.1306/74D719D3-2B21-11D7-8648000102C1865D

Taylor, I.E. and Middleton, G.V., 1990, Aeolian sandstone in the Copper Harbor Formation, Late Proterozoic, Lake Superior basin, Canadian Journal of Earth Science, v. 27, p. 1339-1347. doi.org/10.1139/e90-144

Trewin, N.H., 1993, Controls on fluvial deposition in mixed fluvial and aeolian facies within the Tumblagooda Sandstone (Late Silurian) of Western-Australia, Sedimentary Geology, v. 85, p. 387–400. doi.org/10.1016/0037-0738(93)90094-L

Van Wagoner, J.C., Mitchum, R.M., Campion, K.M. and Rahmanian, V.D., 1990, Siliciclastic Sequence Stratigraphy in Well Logs, Cores, and Outcrops: Concepts for High-Resolution Correlation of Time and Facies, Tulsa, Oklahoma, American Association for Petroleum Geologists Methods in Exploration Series v. 7, p. 1-55. doi.org/10.1306/Mth7510

Vanden Berg, M. D. and Jarrard, R.D., 2004, Cenozoic mass accumulation rates in the equatorial Pacific based on high-resolution mineralogy of Ocean Drilling Program Leg 199, Paleoceanography, 19, PA2021. doi.org/10.1029/2003PA000928

Veiga, G.D., Spalletti, L.A. and Flint, S.S., 2002, Aeolian/fluvial interactions and high-resolution sequence stratigraphy of a non-marine lowstand wedge: the Avile Member of the Agrio Formation (Lower Cretaceous), central Neuquen Basin, Argentina, Sedimentology, v. 49, p. 1001-1019. doi.org/10.1046/j.1365-3091.2002.00487.x

Voss, R., 2002, Cenozoic stratigraphy of the southern Salar de Antofalla region, northwestern Argentina, Revista geológica de Chile, v. 29, p. 167-189. doi.org/10.4067/S0716-02082002000200002

Wanless, H.R. and Shepard, F.P., 1936, Sea level and climatic changes related to late Paleozoic cycles, Geological Society of America Bulletin, v. 47, p. 1177–1206.
doi.org/10.1130/GSAB-47-1177

West, R.R., Archer, A.W. and Miller, K.B., 1997, The role of climate in stratigraphic patterns exhibited by Late Paleozoic rocks exposed in Kansas, Palaeogeography, Palaeoclimatology, Palaeoecology, v. 128, p. 1–16.
doi.org/10.1016/S0031-0182(97)81127-3

Westerhold, T., Röhl, U., Donner, B., McCarren, H. K. and Zachos, J. C., 2011, A complete high-resolution Paleocene benthic stable isotope record for the central Pacific (ODP Site 1209), Global Biogeochemistry, v. 25, p. 1–13.
doi.org/10.1029/2010PA002092

Wilson, I. G., 1971, Desert sandflow basins and a model for the development of ergs. The Geographical Journal, v. 137, p. 180-199.
doi.org/10.2307/1796738

Wilson, I. G., 1973, Ergs, Sedimentary Geology, v. 10, p. 77-106.
doi.org/10.1016/0037-0738(73)90001-8

Winckler, G., Anderson, R.F., Fleisher, M.Q., McGee, D., and Mahowald, N., 2008, Covariant glacial-interglacial dust fluxes in the equatorial Pacific and Antarctica, Science, v. 320, p. 93–96.
doi.org/10.1126/science.1150595.

Withjack, M.O., Schlische R.W., Olsen P.E., 2002, Rift-basin structure and its influence on sedimentary systems, in Renaut, R.W. and Ashley G.M., ed., Sedimentation in Continental Rifts, Society for Sedimentary Geology, Special Publication 73.
doi.org/10.2110/pec.02.73

Woodard, S.C., Thomas, D.J., Hovan, S., Röhl, U. and Westerhold, T., 2011, Evidence for orbital forcing of dust accumulation during the early Paleogene greenhouse, Geochemistry, Geophysics, Geosystems, v. 12, Q02007.
doi.org/10.1029/2010GC003394

Zavala, C. and Freije, R.H., 2001, On the understanding of aeolian sequence stratigraphy: An example from Miocene-Pliocene deposits in Patagonia, Argentina, Rivista Italiana di Paleontologia e Stratigrafia, v. 107, p. 251-264.
doi.org/10.13130/2039-4942/5435

Ziegler, A.M., Scotese, C.R. and Barrett, S.F., 1983, Mesozoic and Cenozoic paleogeographic maps, in Brosche, P. and Sundermann, J., eds., Tidal friction and the earth's rotation. II: Springer, Verlag, Berlin, p. 240-252.
doi.org/10.1007/978-3-642-68836-2_17

FIGURE CAPTIONS

1. A) Distribution of case studies used in this investigation, coloured according to icehouse (blue) and greenhouse (orange) conditions (this colour scheme applies throughout this account). The shape of the marker indicates the paleosupercontinental setting of the case study. B) Geological time-scale showing the five major icehouse periods (labelled A-E) and the distribution of the supercontinents. For all icehouse case-studies, the marker contains a letter (A-E) denoting the associated icehouse period.

2. Factors commonly associated with icehouse and greenhouse conditions. Boxes A-E are theoretical. F) Low latitude sea surface temperatures (based on estimates in Forster et al., 2007). G) Estimates of pCO2 (based on values in Shaviv and Veizer, 2003). H) Pole to equator thermal contrast. I) Planetary windbelt speed (V = velocity). J) Wind shear (V^2= wind velocity squared). K) Wind erosive power (V^3= wind velocity cubed). Boxes H-K are based on the estimates of Kidder and Worsley (2010); the units for boxes I-K are expressed as fractions of the maximum (e.g., 0.67 would be 2/3 of the maximum). Figure adapted in part from Kidder and Worsley (2012).
3. Percentages of: A) eolian and non-eolian architectural elements, B) dune set, sandsheet and interdune elements, and C) non-aeolian elements, deposited under icehouse and greenhouse conditions. Percentages of eolian and non-eolian architectural elements are determined based on total element counts. For descriptions of eolian and non-eolian architectural element types see Table 2.
4. Box and whisker plots showing distributions in element thickness for icehouse and greenhouse conditions: A) all eolian elements; B) dune sets; C) sandsheets; D) interdunes; E) all eolian facies. For descriptions of eolian architectural element types see Table 2.
5. Percentages of: A) wet, dry, and damp interdunes; and the distribution of facies in B) interdunes and C) sandsheets. The percentages are determined based on the total element count. For descriptions of interdune types and facies element types see Table 2.
6. Box and whisker plots of icehouse and greenhouse textural properties. A) modal grain-size; B) sorting; C) grain roundness.
7. Percentages of supersurface descriptions. A) Bypass and deflation surfaces; B) surface 'wetness'; C) surface stabilization. Percentages are calculated based on numbers of occurrences in vertical sections. For full descriptions of surface types and associated attributes see Table 2.
8. Box and whisker plots of element thickness for elements grouped by: A) Proterozoic and Pangean paleosupercontinental settings; B) rift, foreland and intracratonic basin settings; for descriptions of basin types see Table 2; C) different paleolatitudes; and D) different dune-field physiographic settings.
9. Scatterplot showing values of icehouse and greenhouse eolian element thicknesses for different paleolatitudes with mean and median overlain.

10. Cycles of eolian accumulation and deflation under icehouse glacials and interglacials with accompanying sequence stratigraphic terminology. A) Deposition of thin sandsheet and dune-set elements associated with the onset of glacial conditions. B) Deposition of thick dune sets associated with strong trade-wind strengths and high rates of sediment supply in an arid setting. Both A and B show a relative fall in the level of the water table. C) Onset of deflation as a sediment source is exhausted. D) As interglacial conditions proceed, deflation continues to the level of the water table. Both C and D show a rise in the relative level of the water table, associated with more humid interglacial conditions. The rise in the level of the water table protects the lower part of the aeolian succession from erosion. E-G the start of a new glacial/interglacial cycle. The indicative lateral and vertical scales in Part A apply to all box models.
11. Deposition of an eolian sequence under greenhouse conditions. The temporal sediment supply remains relatively static (A-D). An elevated water table associated with relatively humid conditions promotes the preservation of eolian dune sets by protecting them from potential wind erosion; accumulated dune sets are sequestered into the geological record (B-D). The generation of supersurfaces is most likely to be associated with fluvial inundation or due to a transition from eolian to sabkha deposition (C). The indicative lateral and vertical scales in Part A apply to all box models.
12. Percentages of different basin-setting types (continental rift, foreland and intracratonic) for Proterozoic age case studies, subdivided into icehouse and greenhouse conditions.
13. Box and whisker plots showing eolian architectural element thicknesses for Proterozoic, Pangean and Gondwanaland paleosupercontinenal settings.

TABLE CAPTIONS

1. List of the case studies used in this investigation. The geographic location of each case study is outlined in Figure 1 (identified via the case number). The reference refers to the original source material from which quantitative metrics were derived.
2. Definitions of eolian and non-eolian architectural element types, facies element types, surface types, and basin types discussed in the text.

3. Results of statistical analysis; SD: standard deviation; P(T<=t): one tail t-test; ANOVA: analysis of variance. All results are reported to two decimal places, where appropriate. For all statistical calculations see Supplementary Information.

Figure 1

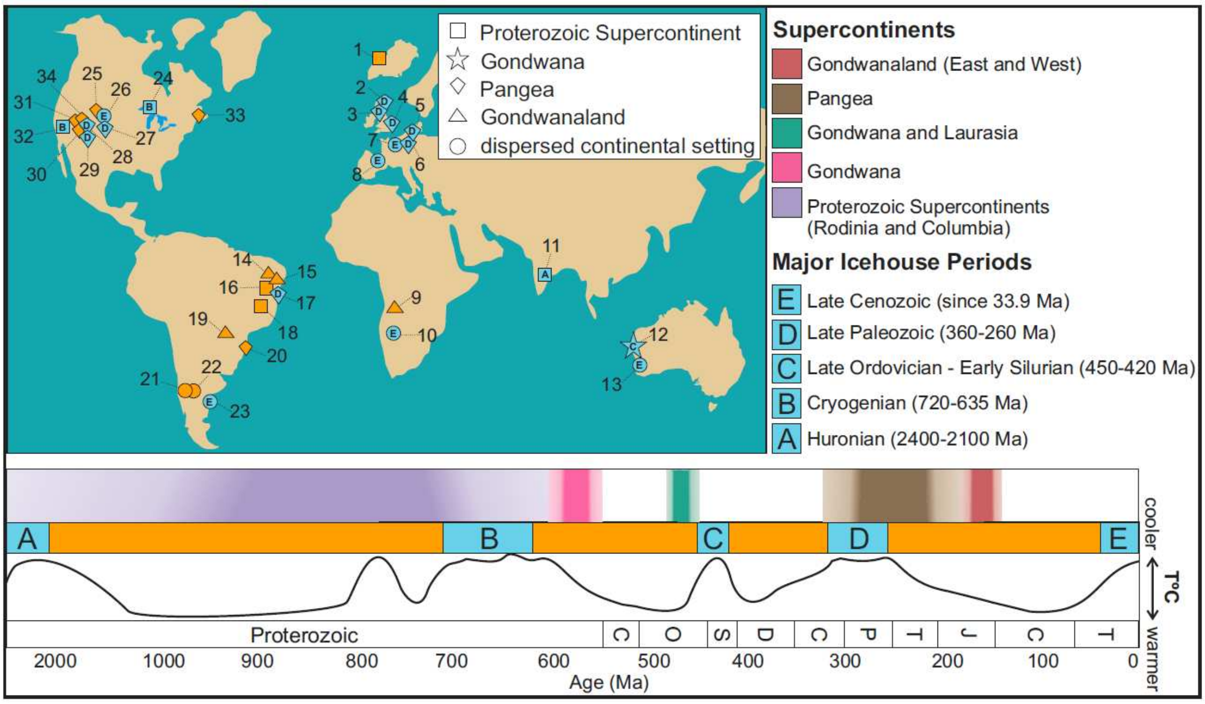

Figure 2

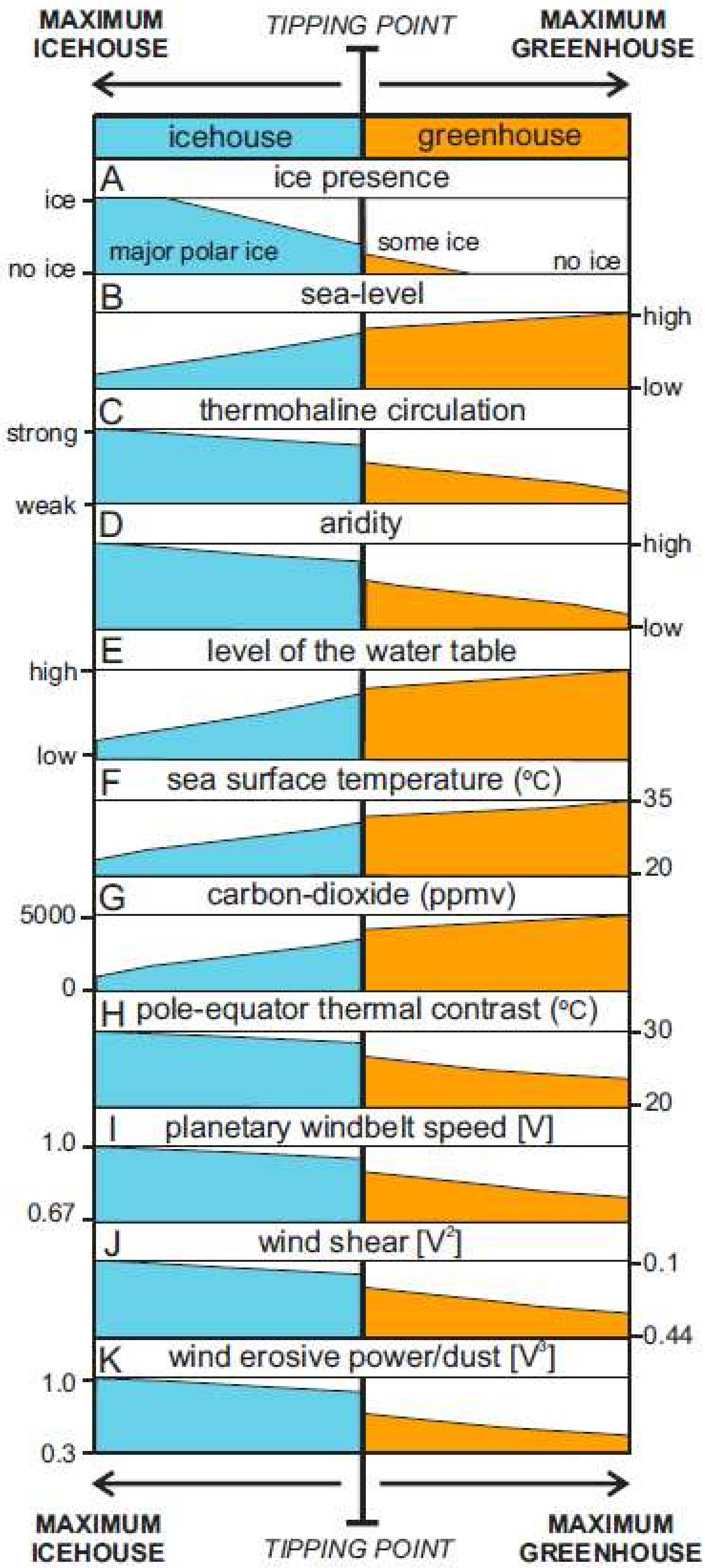
MAXIMUM ICEHOUSE
TIPPING POINT
MAXIMUM GREENHOUSE
icehouse
greenhouse
A ice presence
ice
no ice
major polar ice
some ice
no ice
B sea-level
high
low
C thermohaline circulation
strong
weak
D aridity
high
low
E level of the water table
high
low
F sea surface temperature (°C)
35
20
G carbon-dioxide (ppmv)
5000
0
H pole-equator thermal contrast (°C)
30
20
I planetary windbelt speed [V]
1.0
0.67
J wind shear [V²]
0.1
0.44
K wind erosive power/dust [V³]
1.0
0.3
MAXIMUM ICEHOUSE
TIPPING POINT
MAXIMUM GREENHOUSE

Figure 3

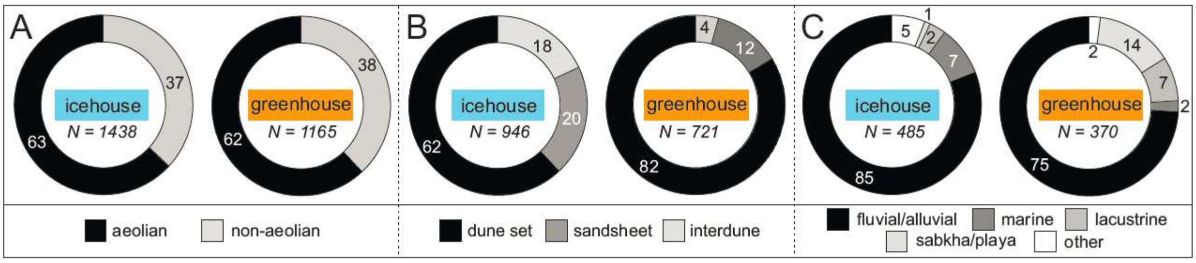

Figure 4

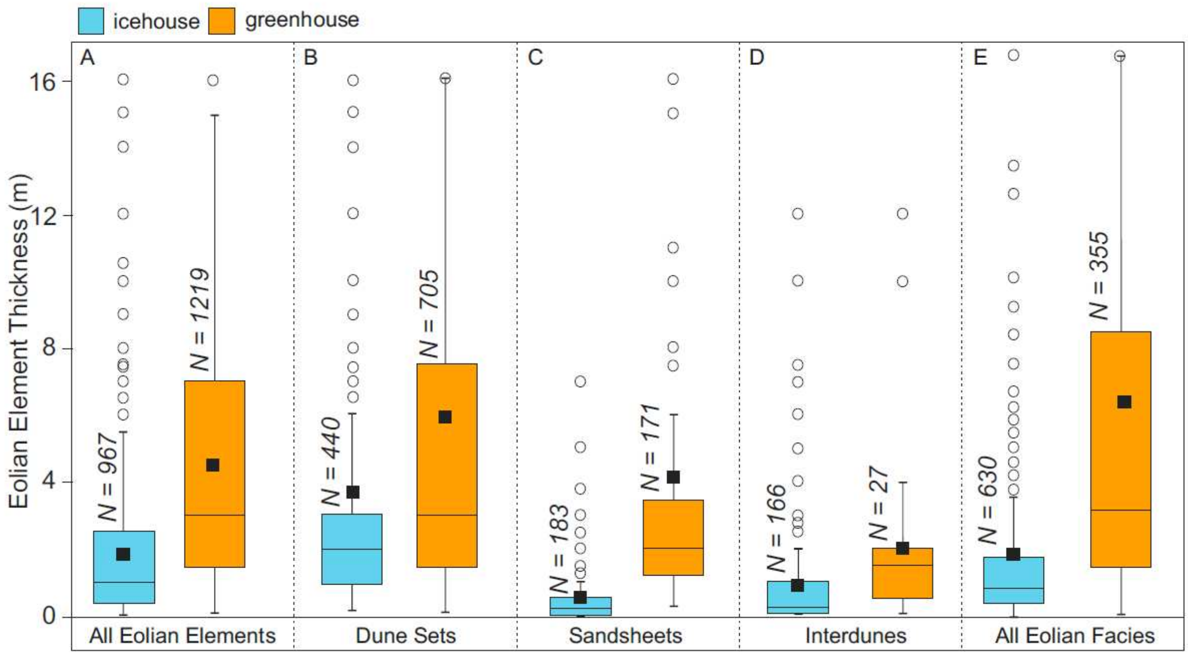

Figure 5

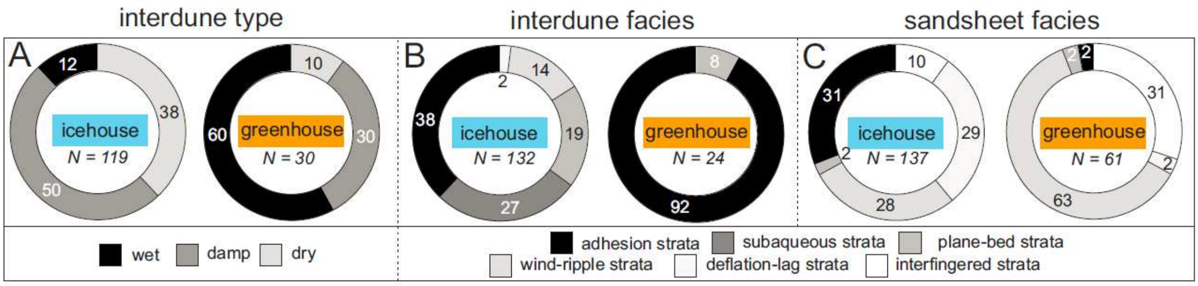

Figure 6

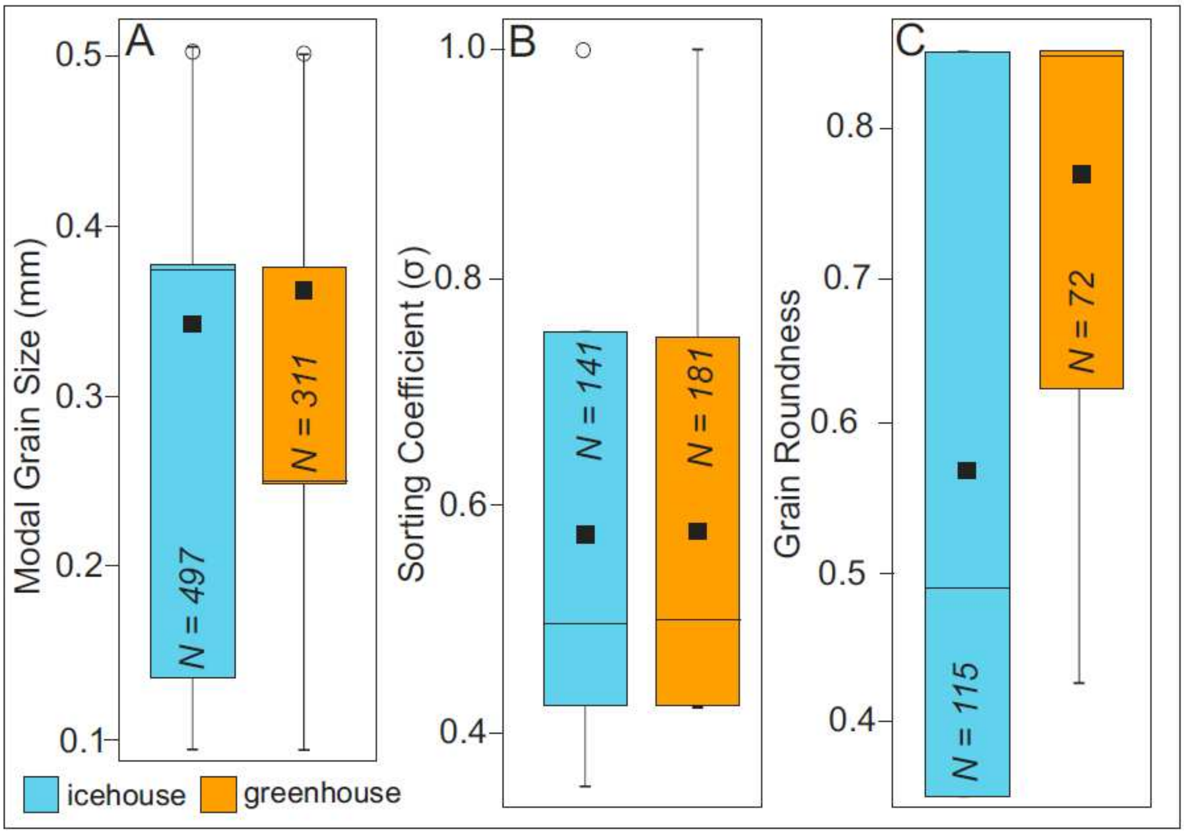

Figure 7

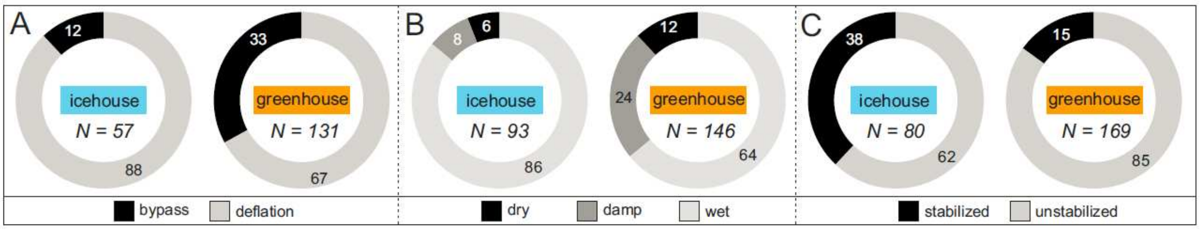

Figure 8

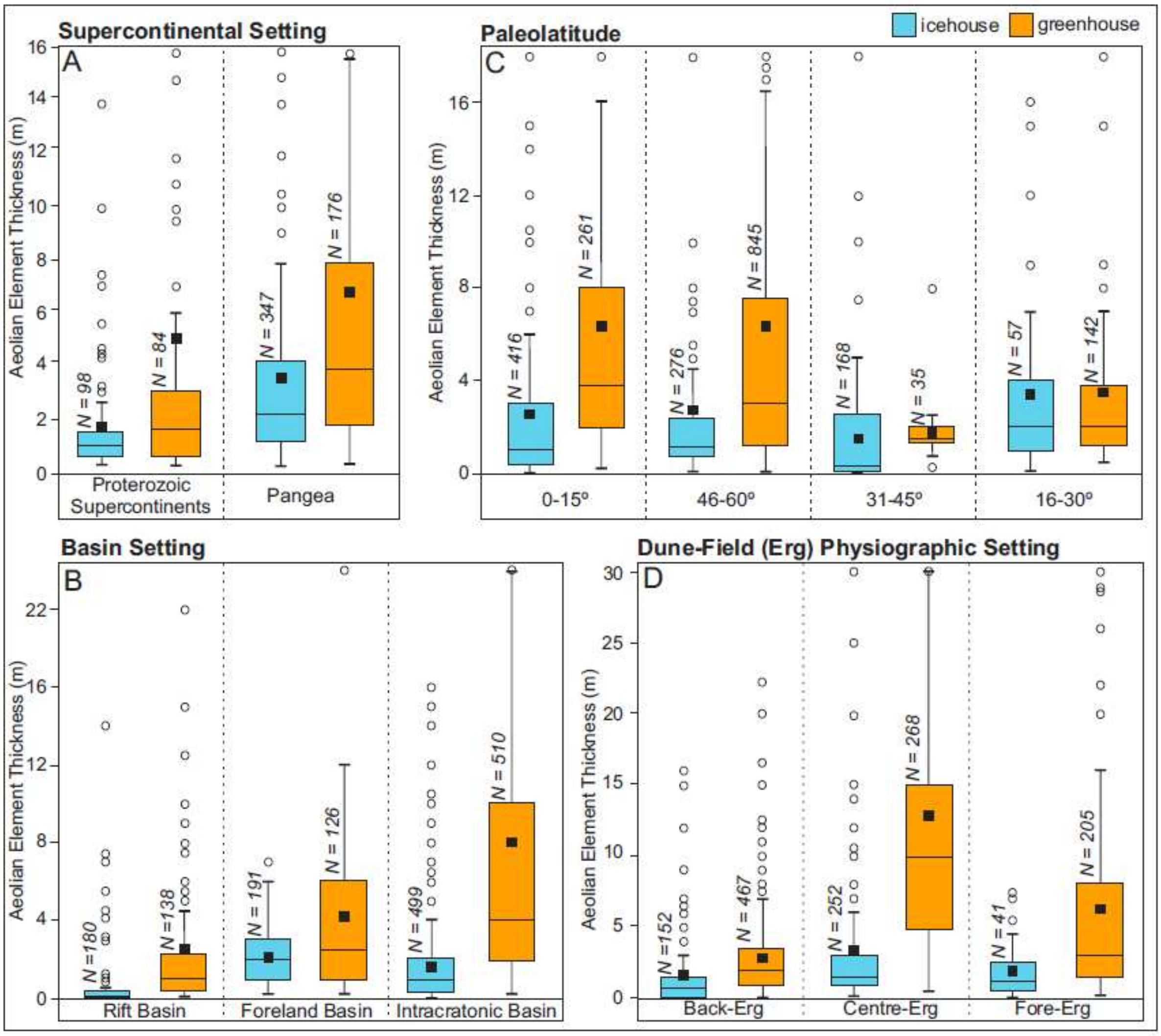
Supercontinental Setting
A
Aeolian Element Thickness (m)
N = 98
N = 84
N = 347
N = 176
Proterozoic Supercontinents
Pangea
Paleolatitude
C
icehouse
greenhouse
N = 416
N = 261
N = 276
N = 845
N = 168
N = 35
N = 57
N = 142
0-15º
46-60º
31-45º
16-30º
Basin Setting
B
N = 180
N = 138
N = 191
N = 126
N = 499
N = 510
Rift Basin
Foreland Basin
Intracratonic Basin
Dune-Field (Erg) Physiographic Setting
D
N = 152
N = 467
N = 252
N = 268
N = 41
N = 205
Back-Erg
Centre-Erg
Fore-Erg

Figure 9

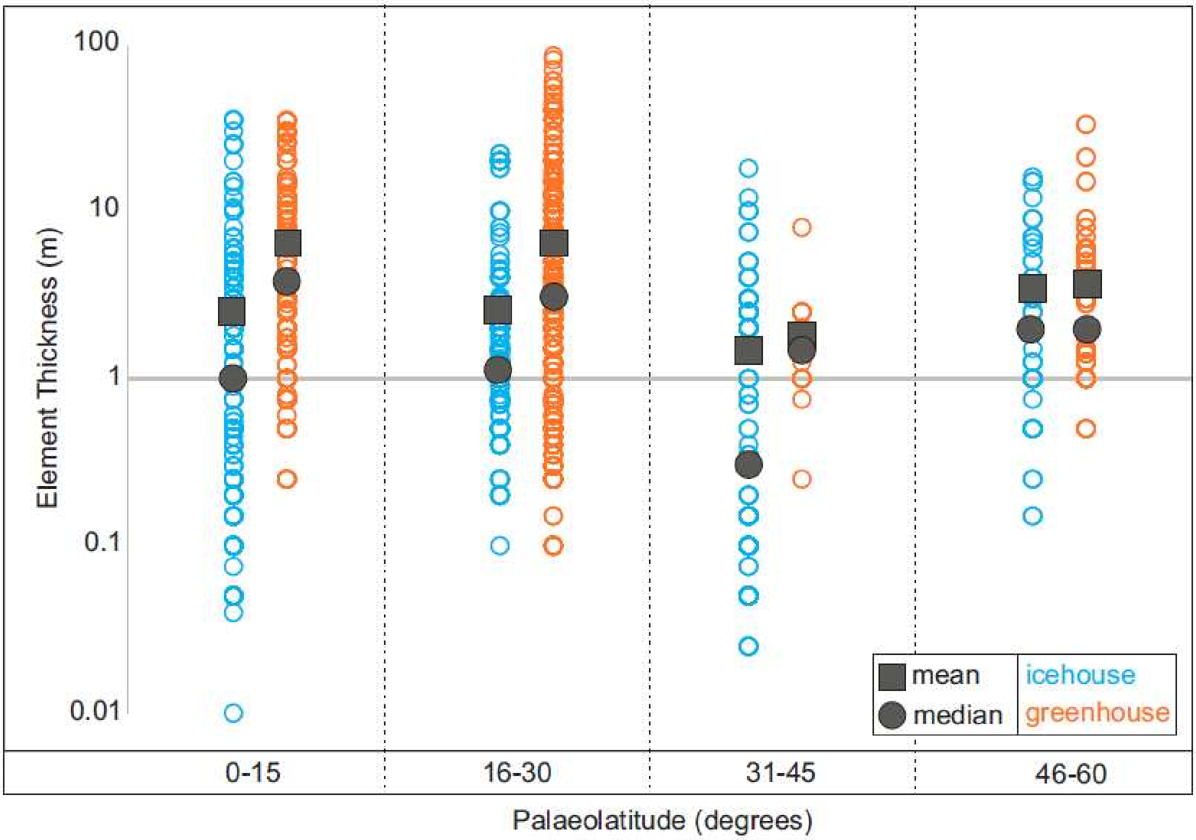
100
10
1
0.1
0.01
Element Thickness (m)
mean
median
icehouse
greenhouse
0-15
16-30
31-45
46-60
Palaeolatitude (degrees)

Figure 10

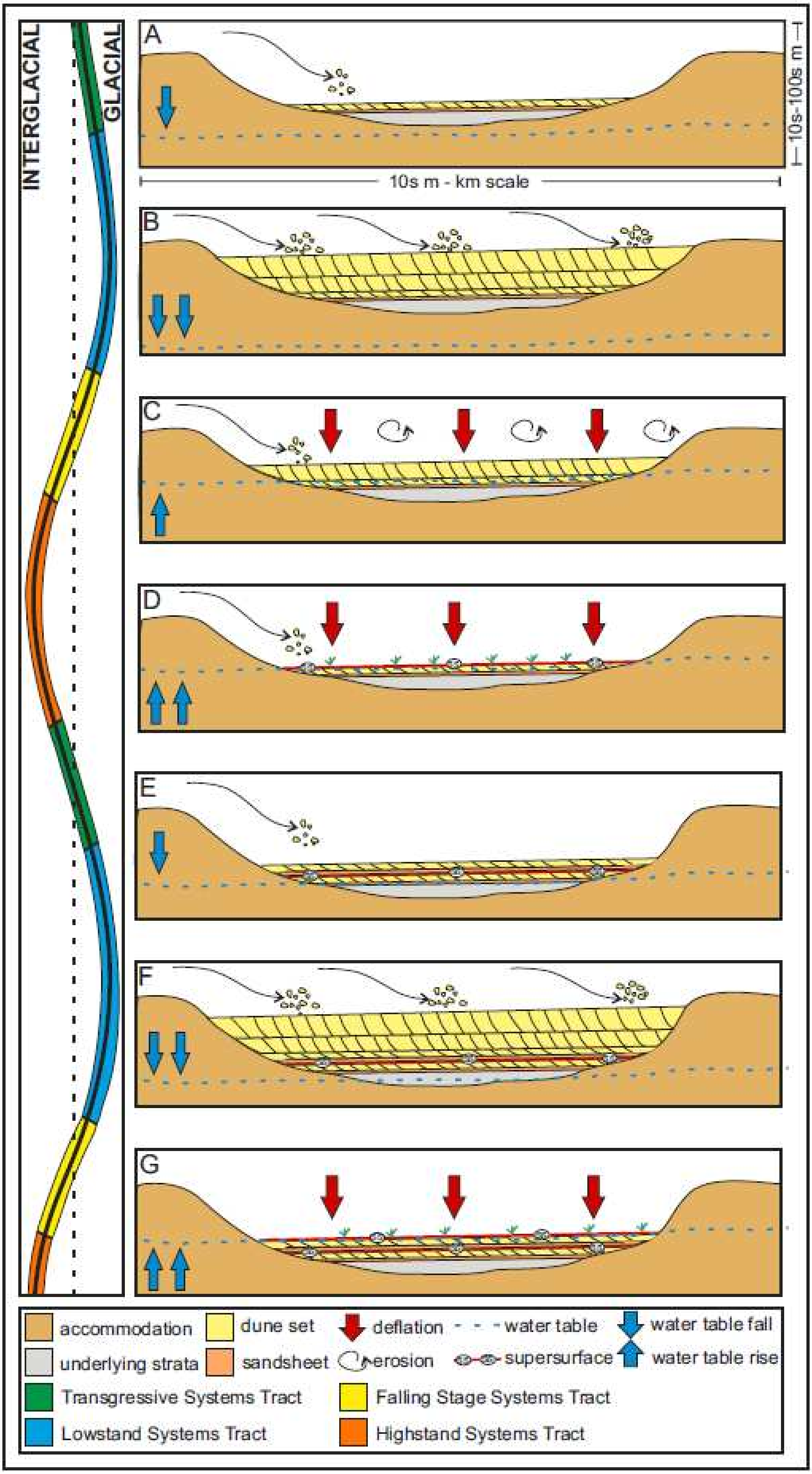
INTERGLACIAL
GLACIAL
A
10s-100s m
10s m - km scale
B
C
D
E
F
G
accommodation
dune set
deflation
water table
water table fall
underlying strata
sandsheet
erosion
supersurface
water table rise
Transgressive Systems Tract
Falling Stage Systems Tract
Lowstand Systems Tract
Highstand Systems Tract

Figure 11

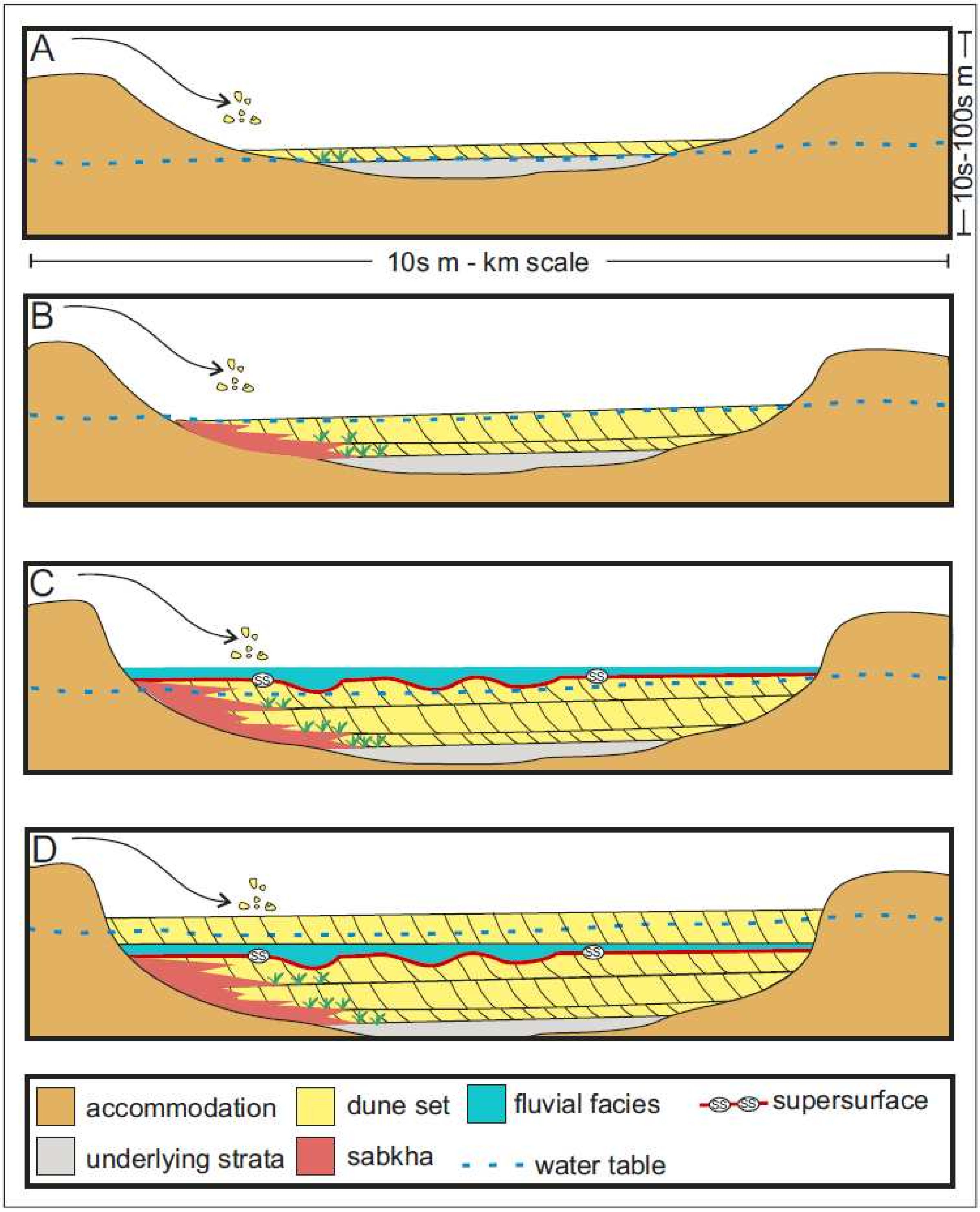
A
B
C
D
10s-100s m
10s m - km scale
SS
accommodation
underlying strata
dune set
sabkha
fluvial facies
water table
supersurface

Figure 12

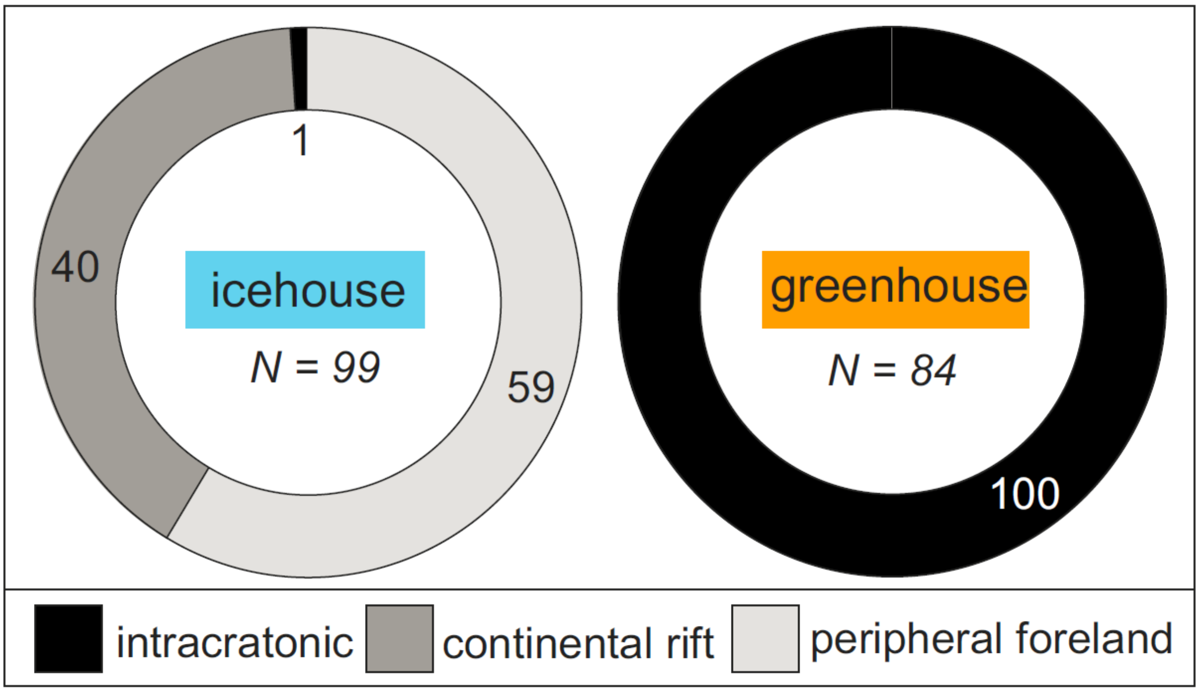
1
40
icehouse
N = 99
59
greenhouse
N = 84
100
intracratonic
continental rift
peripheral foreland

Figure 13

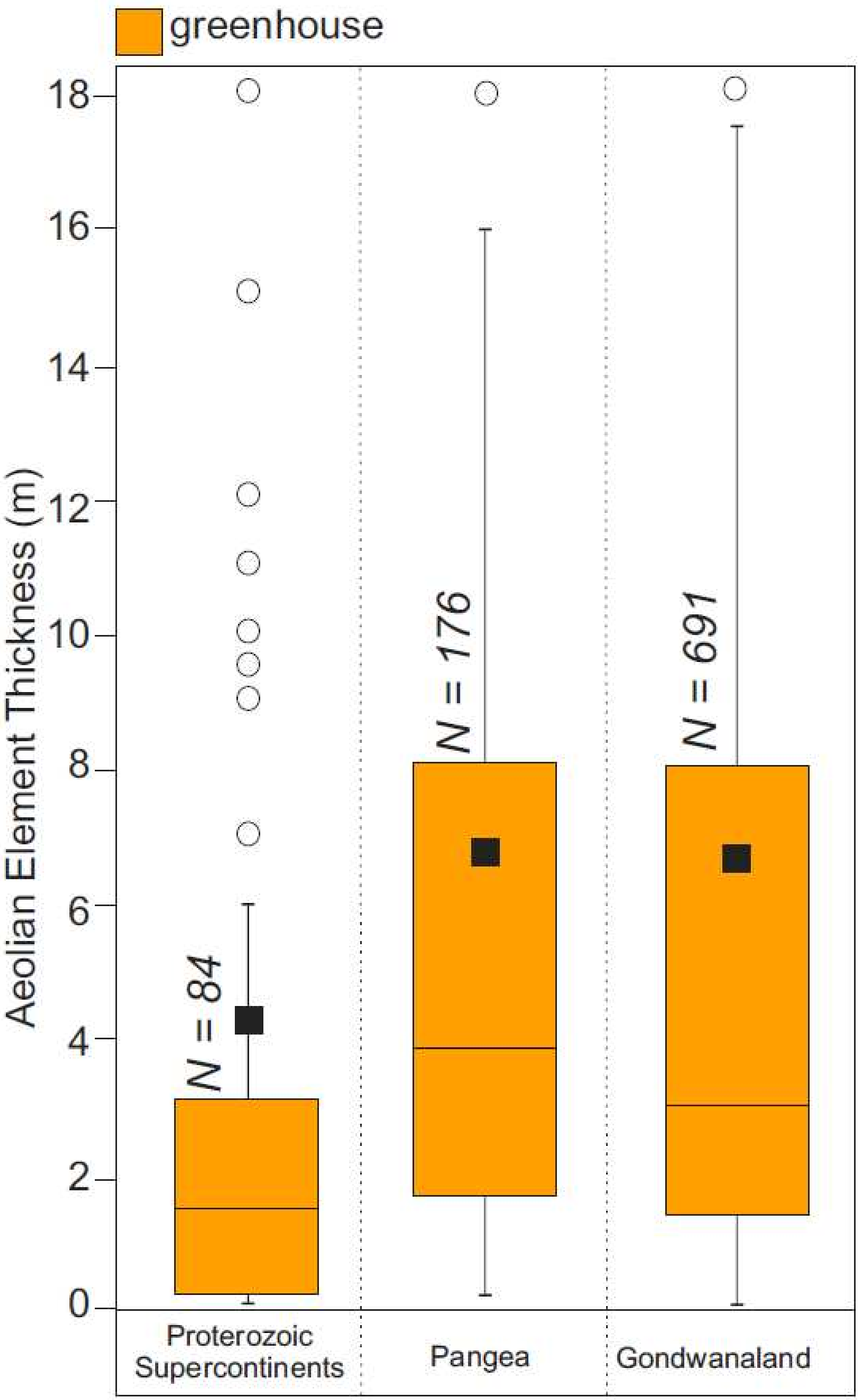
greenhouse
Aeolian Element Thickness (m)
0
2
4
6
8
10
12
14
16
18
N = 84
N = 176
N = 691
Proterozoic Supercontinents
Pangea
Gondwanaland

Table 1: Case study details					
Case Number	Icehouse or Greenhouse	Age (Ma)	Case Study Name	Location	Reference(s)
1	Greenhouse	ca. 1320 - 1000	Eriksfjord Formation	Greenland	Clemmenesen (1988)
2	Icehouse	ca. 259 - 254	Hopeman Sandstone	Scotland, UK	Clemmensen (1987)
3	Icehouse	ca. 290 - 240	Arran Red Beds	Isle of Arran, Scotland, UK	Clemmensen and Abrahamsen (1983)
4	Icehouse	ca. 252 - 242	Sherwood Sandstone	UK (Onshore and Offshore England and Northern Ireland)	Cowan (1993); Meadows and Beach (1993)
5	Icehouse	ca. 299 - 252	Rotliegendes Sandstone	Germany, Poland, Denmark, Baltic Sea, Netherlands	Ellis (1993); Newell (2001)
6	Icehouse	< 1	Boxtel Formation	Netherlands, Germany, Denmark, Poland	Schokker and Koster (2004)
7	Icehouse	ca. 38 - 34	Sable de Fontainbleau Formation	France	Cojan and Thiry (1992)
8	Icehouse	ca. 5	Escorihuela Formation	NE Spain	Liesa et al. (2016)
9	Greenhouse	ca. 132	Etjo Formation	Namibia	Mountney and Howell (2000)
10	Icehouse	ca. 23 - 3	Tsondab Sandstone	Namibia	Kocurek et al. (1999)
11	Icehouse	ca. 1400 - 1327	Egalapenta Formation	India	Biswas (2005); Dasgupta et al. (2005)
12	Greenhouse	ca. 430 - 420	Tumblagooda Formation	Australia	Trewin (1993)
13	Icehouse	ca. 3	Tamala Limestone	Australia	Semeniuk and Glassford (1988)
14	Greenhouse	ca. 140 - 125	Sao Sebastio Formation	Brazil	Formola Ferronatto et al. (2019)
15	Greenhouse	ca. 148 - 144	Sergi Formation	Brazil	Scherer et al. (2007)
16	Greenhouse	ca. 1800 - 1600	Mangabeira Formation	Brazil	Ballico et al. (2017)
17	Icehouse	ca. 298 - 272	Caldeirao Formation	Brazil	Jones et al. (2015)
18	Greenhouse	ca. 1800 - 1700	Bandeirinha Formation	Brazil	Simplicico and Basilici (2015)
19	Greenhouse	ca. 163 - 145	Guara Formation	Brazil	Scherer and Lavina (2005)
20	Icehouse	ca. 260 - 257	Piramboia Formation	Brazil	Dias and Scherer (2008)
21	Greenhouse	ca. 129 - 125	Huitrin Formation	Argentina	Strömbäck et al. (2005)
22	Greenhouse	ca. 130 - 129	Agrio Formation	Argentina	Viega et al. (2002)
23	Icehouse	ca. 10 - 4	Rio Negro Formation	Argentina	Zavala and Frieje (2001)
24	Icehouse	ca. 720 - 640	Copper Habor Formation	Michigan, USA	Taylor and Middleton (1990)
25	Greenhouse	ca. 250 - 245	Chugwater Formation	Wyoming, USA	Irmen and Vondra (2000)

26	Icehouse	ca. 23 - 16	Arikaree Formation	Wyoming, Nebraska, USA	Bart (1977)
27	Icehouse	ca. 299 - 280	Ingleside Formation	Colorado, Wyoming, USA	Pike and Sweet (2018)
28	Icehouse	ca. 299- 280	Lower Cutler Beds	Utah, USA	Jordan and Mountney (2010)
29	Icehouse	ca. 286 - 245	Cedar Mesa Sandstone	Utah, Colorado, New Mexico, Arizona, USA	Loope (1985); Mountney and Jagger (2004); Mountney (2006)
30	Greenhouse	ca. 201 - 191	Navajo Sandstone	Nevada, Arizona, Colorado, Utah, USA	Loope and Rowe (2003)
31	Greenhouse	ca. 166 - 163	Entrada Sandstone	Wyoming, Utah, Arizona, New Mexico, Texas, USA	Crabaugh and Kocurek (1993); Benan and Kocurek (2000); Kocurek and Day (2018)
32	Icehouse	ca. 1000 - 750	Big Bear Formation	California, USA	Stewart (2005)
33	Greenhouse	ca. 227 - 210	Wolfville Formation	Nova Scotia, Canada	Leleu and Hartley (2018)
34	Greenhouse	ca. 170 - 166	Page Sandstone	Arizona, Utah, Wyoming, USA	Jones and Blakey (1997); Kocurek et al. (1992)

Table 2: List of definitions used in the text

Eolian Architectural Element Types	
Cross-strata package	Packages of aeolian stratification (typically composed of wind-ripple, grainflow and grainfall strata; Hunter 1977, 1981); form parts of dune sets; packages of cross-strata are typically separated by reactivation surfaces (Brookfield, 1977; Kocurek, 1996).
Dune set	Dune-sets form the fundamental unit of deposition of an eolian sand dune; dune-sets are formed of packages of cross-strata (Sorby, 1859; Allen, 1963; Rubin and Hunter 1982; Chrintz and Clemmensen, 1993); if dune sets migrate over each other, cross-stratified packages are truncated, delineating sets that are bounded by erosional surfaces (Brookfield, 1977; Kocurek, 1996).
Dune coset	Two or more genetically related dune sets that occur in vertical succession; both the coset and its contained sets are separated by bounding surfaces (Brookfield, 1977; Kocurek, 1996).
Dune compound set	A specialized class of coset wherein the contained sets record the migration of formative bed forms of a common type, for example where dunes migrate over the flanks of a parent megabedform (draa) which is itself migrating to leave an accumulation; both the compound set and its contained sets are separated by bounding surfaces (Brookfield, 1977; Kocurek, 1996).
Sandsheet	Sandsheet deposits are low-relief accumulations of eolian sediment in areas where dunes are generally absent (Nielsen and Kocurek, 1986; Brookfield, 1992; Rodríguez-López et al., 2012); sandsheets can also comprise low-relief bedforms such as zibars.
Interdune	Interdune deposits are formed in the low-relief, flat, or gently sloping areas between dunes; neighboring dunes are separated by interdunes (Hummel and Kocurek, 1984).
Dry interdune	Dry interdunes are characterized by deposits that accumulate on a substrate where the water table is well below the ground surface, such that sedimentation is not controlled by and is largely not influenced by the effects of moisture (Fryberger et al., 1990).
Damp interdune	Damp interdunes are characterized by deposits that accumulate on a substrate where the water table is close to the ground surface, such that sedimentation is influenced by the presence of moisture (Fryberger et al., 1988; Lancaster and Teller, 1988; Kocurek et al., 1992).

Wet interdune	Wet interdunes are characterized by deposits that accumulate on a substrate where the water table is elevated above the ground surface such that the interdune is episodically or continuously flooded with water (Kocurek and Havholm, 1993; Loope et al., 1995; García-Hidalgo et al., 2002).
Eolian Facies Element Types	
Wind-ripple strata	Wind-ripple lamination forms when wind-blown, saltating grains strike sand-grains obliquely and propel other grains forward (Bagnold, 1941; Hunter, 1977). The foreset laminae of wind-ripple strata are occasionally preserved (rippleform laminae), however, the internal laminae of wind-ripple strata are often indistinguishable due to grain size uniformity (translatent wind-ripple stratification; Hunter, 1977).
Grainflow strata	Grainflow strata form where a dune slipface undergoes gravitational collapse (Hunter, 1977; Bristow and Mountney, 2013). Grainflow deposits are typically erosionally based and are devoid of internal structure, forming discrete tongues or wide sheets of inclined strata on the lee-slope of dunes, which wedge-out towards the base of the dune. Individual grainflow strata may be indistinguishable, resulting in amalgamated grainflow units (Howell and Mountney, 2001).
Grainfall strata	Grainfall strata are gravity-driven deposits that occur when the wind transports saltating clouds of grains beyond a dune brink; grains settle onto the upper portions of lee slopes as wind transport capacities reduce in the lee-side depressions (Nickling et al., 2002). Grainfall laminae are typically thin (<1 mm), drape existing topography, else may have a wedge-shaped geometry; grainfall lamination is generally composed of sand and silt or (rarely) clay sizes grains (Hunter, 1977).
Interfingered strata	Interfingered strata represent intercalated packages of wind-ripple, grainflow, grainfall and plane-bed strata; two or more of the aforementioned stratal types may be present. This composite facies type is used only in cases where it is not possible to differentiate individual wind-ripple, grainflow, grainfall or plane-bed facies elements. Interfingered strata can occur in a variety of eolian settings and are especially common on dune lee slopes (Hunter, 1977; Hunter, 1981).
Adhesion strata	Adhesion strata results from the adhesion of moving grains to a damp surface, such as a damp interdune (Hummel and Kocurek, 1984). Adhesion strata typically are low relief (several mm in height) and exhibit sub-horizontal structures with irregular surfaces. Adhesion strata can comprise adhesion plane beds, adhesion ripples (Kocurek and Fielder, 1982) and adhesion warts (Olsen et al., 1989).
Plane-bed strata	Plane-bed lamination forms when wind velocities are too high to form ripples (Hunter 1977, 1981). Plane-bed lamination is composed of (sub)horizontally laminated sand, which typically dips at angles of between 0 and 15° (Pye, 2009). Plane-bed laminae are typically millimeter-scale, with sharp or gradational contacts (e.g., Clemmensen and Abrahamsen, 1983) and form sets typically up to 100 mm (Pye, 2009).
Subaqueous ripple strata	Subaqueous ripple lamination is generated by tractional processes and are produced by the action of waves or currents on a sediment surface (Allen, 1978).
Non-Eolian Element Types	
Fluvial/Alluvial	Deposits arising from or relating to the action of rivers/streams and sediment gravity-flow processes (cf. Melton, 1965).
Marine	Deposits arising from or relating to accumulation in marine environments.
Lacustrine	Deposits arising from or relating to accumulation in perennial lakes.
Sabkha/Playa	Sabkhas and playa lakes describe low-relief flats where evaporites, and in some cases carbonates, accumulate. The terms sabkha and playa lake were originally used to describe coastal and inland settings, respectively (Evans, et al., 1964; Purser and Evans, 1973); however, the terms are now commonly used interchangeably.
Other	Any depositional element that differs in origin from those above.
Surface Types	
Supersurface	Surfaces resulting from the cessation of eolian accumulation; occurs where the sediment budget switches from positive to negative (cannibalization of eolian system) or neutral (zero angle of climb), resulting in deflation (*deflationary supersurface*) or bypass (*bypass supersurface*) of the eolian system, respectively. Supersurfaces are also generated by changes in depositional environment, such as transition from eolian to fluvial, or eolian to marine deposition (e.g., Glennie and Buller, 1983; Chan and Kocurek, 1988).
Wet-type supersurface	Supersurface associated with deflation down to the water-table (also known as a Stokes surface). Wet-type supersurfaces may be associated with aqueous inundation by a non-eolian source (e.g., fluvial/marine deposits).

Damp-type supersurface	Supersurface associated with bypass/deflation; the level of the water table is interacting with the surface.
Dry-type supersurface	Supersurface associated with bypass/deflation; the level of the water table is significantly below the surface.
Basin Types	
Intracratonic (sag) basins	An intracratonic (sag) basin is a depressed or persistently low area occurring in the interior of cratonic blocks or on stable continental crust (Middleton, 1989); they are characterized by generally low rates of accommodation generation, and host sedimentary infills that can be >10 km in thickness and that typically embody over 200-800 Myr (Einsele, 2013).
Rift basin	A continental rift is an elongate graben or half-graben trough (ca. 10^3-10^4 km^2) bounded by normal faults, associated with active lithospheric extension and thinning (Gregory, 1894); rift basins are characterized by high rates of accommodation generation (e.g., Rosendahl, 1987; Schlische, 1993; Morley, 1995; Withjack et al., 2002).
Foreland basins	A foreland basin is here defined as a depression generated by flexure of the continental crust in front of a fold-and-thrust mountain belt (Einsele, 2013) and are characterized by intermediate rates of accommodation generation.

Table 3: Results of statistical analyses						
ARCHITECTURAL AND FACIES ELEMENT THICKNESS						
	EOLIAN ARCH. EL.		*NON-EOLIAN ARCH. EL.*		*FACIES ELEMENTS*	
	ICEHOUSE	GREENHOUSE	ICEHOUSE	GREENHOUSE	ICEHOUSE	GREENHOUSE
MEAN	2.36	5.47	5.18	4.88	2.20	7.53
MEDIAN	1.00	2.50	2.00	2.00	1.00	3.75
SD	4.48	8.40	10.07	12.24	3.93	10.23
N	789	903	367	519	630	355
P(T<=t)	0.00		0.35		0.00	
SIGNIFICANT?	TRUE		FALSE		TRUE	
SPECIFIC EOLIAN ELEMENTS						
	DUNE SET		*SANDSHEET*		*INTERDUNE*	
	ICEHOUSE	GREENHOUSE	ICEHOUSE	GREENHOUSE	ICEHOUSE	GREENHOUSE
MEAN	3.67	5.93	0.55	4.15	0.88	2.00
MEDIAN	2.00	3.00	0.20	2.00	0.25	1.50
SD	5.54	7.94	0.88	10.33	1.74	2.75
N	440	705	183	171	166	27
P(T<=t)	0.00		0.00		0.00	
SIGNIFICANT?	TRUE		TRUE		TRUE	
EOLIAN TEXTURE						
	GRAIN SIZE		*SORTING*		*ROUNDNESS*	
	ICEHOUSE	GREENHOUSE	ICEHOUSE	GREENHOUSE	ICEHOUSE	GREENHOUSE
MEAN	0.34	0.36	0.57	0.58	0.57	0.77

MEDIAN	0.38	0.25	0.50	0.50	0.49	0.85
SD	0.27	0.25	0.19	0.19	0.22	0.12
N	496	310	140	179	113	70
P(T<=t)	0.14		0.43		0.00	
SIGNIFICANT?	FALSE		FALSE		TRUE	

EOLIAN ARCHITECTURAL ELEMENTS BY SUPERCONTINENTAL SETTING				
	PROTEROZOIC SUPERCONTINENTS		*PANGEA*	
	ICEHOUSE	GREENHOUSE	ICEHOUSE	GREENHOUSE
MEAN	1.43	5.04	3.41	6.85
MEDIAN	0.80	1.50	2.00	3.86
SD	2.41	14.44	5.31	7.87
N	98	84	347	176
P(T<=t)	0.02		0.00	
SIGNIFICANT?	TRUE		TRUE	

EOLIAN ARCHITECTURAL ELEMENTS BY BASIN SETTING						
	INTRACRATONIC BASIN		*CONTINENTAL RIFT BASIN*		*FORELAND BASIN*	
	ICEHOUSE	GREENHOUSE	ICEHOUSE	GREENHOUSE	ICEHOUSE	GREENHOUSE
MEAN	1.73	7.63	0.70	2.48	2.11	4.23
MEDIAN	1.00	3.50	0.15	1.00	2.00	2.50
SD	2.24	10.77	2.00	3.69	1.44	4.47
N	507	595	138	180	191	126
P(T<=t)	0.00		0.00		0.00	
SIGNIFICANT?	TRUE		TRUE		TRUE	

EOLIAN ARCHITECTURAL ELEMENTS BY PALAEOLATITUDE				
	0-15 DEGREES		*16-30 DEGREES*	
	ICEHOUSE	GREENHOUSE	ICEHOUSE	GREENHOUSE
MEAN	2.60	6.38	2.72	6.40
MEDIAN	1.00	3.75	1.10	3.00
SD	4.84	7.08	4.57	9.82
N	416	261	276	845
P(T<=t)	0.00		0.00	
SIGNIFICANT?	TRUE		TRUE	
	31-45 DEGREES		*46-60 DEGREES*	
	ICEHOUSE	GREENHOUSE	ICEHOUSE	GREENHOUSE

MEAN	1.53	1.75	3.39	3.50
MEDIAN	0.30	1.50	2.00	2.00
SD	2.42	1.21	3.92	4.76
N	168	35	57	142
P(T<=t)	0.30		0.44	
SIGNIFICANT?	FALSE		FALSE	

EOLIAN ARCHITECTURAL ELEMENTS BY ERG DISTALITY

	BACK ERG		*CENTER ERG*		*FORE ERG*	
	ICEHOUSE	GREENHOUSE	ICEHOUSE	GREENHOUSE	ICEHOUSE	GREENHOUSE
MEAN	1.65	2.92	3.39	12.83	1.87	6.36
MEDIAN	0.75	2.00	1.50	10.00	1.20	3.00
SD	2.79	3.22	5.96	11.75	1.81	7.37
N	152	467	252	268	41	205
P(T<=t)	0.00		0.00		0.00	
SIGNIFICANT?	TRUE		TRUE		TRUE	

COMPARISONS OF GREENHOUSE PANGEAN DEPOSITS WITH OTHER GREENHOUSE SUPERCONTINENTAL SETTINGS

	GREENHOUSE ONLY		GREENHOUSE ONLY	
	PANGEA	*GONDWANALAND*	*PANGEA*	*PROTEROZOIC SUP.*
MEAN	6.85	6.70	6.85	4.26
MEDIAN	3.88	3.00	3.88	1.50
SD	7.87	9.43	7.87	12.63
OBSERVATIONS	176	691	176	84
ANOVA	0.85		0.04	
SIGNIFICANT?	FALSE		FALSE	

SUPERSURFACE SPACING

	ICEHOUSE	GREENHOUSE
MEAN	16.34	9.07
MEDIAN	16.00	9.00
SD	12.70	6.34
OBSERVATIONS	25	7